RSC Advances

PAPER

View Article Online
View Journal | View Issue

Cite this: *RSC Adv.*, 2024, **14**, 4005

Innovative microwave-assisted biosynthesis of copper oxide nanoparticles loaded with platinum(II) based complex for halting colon cancer: cellular, molecular, and computational investigations†

Nada K. Sedky, ‡[a] Iten M. Fawzy, ‡[b] Afnan Hassan,[c] Noha Khalil Mahdy,[d] Reem T. Attia,[e] Samir N. Shamma,[f] Mohammad Y. Alfaifi,[g] Serag Eldin Elbehairi,[g] Fatma A. Mokhtar[h] and Sherif Ashraf Fahmy *[i]

In the current study, we biosynthesized copper oxide NPs (CuO NPs) utilizing the essential oils extracted from *Boswellia carterii* oleogum resin, which served as a bioreductant and capping agent with the help of microwave energy. Afterwards, the platinum(II) based anticancer drug, carboplatin (Cr), was loaded onto the CuO NPs, exploiting the electrostatic interactions forming Cr@CuO NPs. The produced biogenic NPs were then characterized using zeta potential (ZP), high-resolution transmission electron microscopy (HRTEM), X-ray diffraction spectroscopy (XRD), and Fourier transform infrared spectroscopy (FTIR) techniques. In addition, the entrapment efficiency and release profile of the loaded Cr were evaluated. Thereafter, SRB assay was performed, where Cr@CuO NPs demonstrated the highest cytotoxic activity against human colon cancer cells (HCT-116) with an IC_{50} of 5.17 μg mL^{-1}, which was about 1.6 and 2.2 folds more than that of Cr and CuO NPs. Moreover, the greenly synthesized nanoparticles (Cr@CuO NPs) displayed a satisfactory selectivity index (SI = 6.82), which was far better than the free Cr treatment (SI = 2.23). Regarding the apoptosis assay, the advent of Cr@CuO NPs resulted in an immense increase in the cellular population percentage of HCT-116 cells undergoing both early (16.02%) and late apoptosis (35.66%), significantly surpassing free Cr and CuO NPs. A study of HCT-116 cell cycle kinetics revealed the powerful ability of Cr@CuO NPs to trap cells in the Sub-G1 and G2 phases and impede the G2/M transition. RT-qPCR was utilized for molecular investigations of the pro-apoptotic (Bax and p53) and antiapoptotic genes (Bcl-2). The novel Cr@CuO NPs treatment rose above single Cr or CuO NPs therapy in stimulating the p53-Bax mediated mitochondrial apoptosis. The cellular and molecular biology investigations presented substantial proof of the potentiated anticancer activity of Cr@CuO NPs and the extra benefits that could be obtained from their use.

Received 22nd December 2023
Accepted 21st January 2024

DOI: 10.1039/d3ra08779d

rsc.li/rsc-advances

Introduction

Colon cancer is the third most frequent cancer worldwide, causing more than 1 million morbidity cases during the last decade.[1] Despite being one of the most diagnosed types of tumors, colon cancer is characterized by high mortality rates due to poor prognosis.[2] The pathogenesis of colon cancer involves genetic mutations, environmental factors, wrong food habits with insufficient nutrients, and improper lifestyle habits, including smoking.[3] Three main conventional treatment

[a]*Department of Biochemistry, School of Life and Medical Sciences, University of Hertfordshire Hosted by Global Academic Foundation, R5 New Garden City, New Administrative Capital, Cairo, Egypt*

[b]*Department of Pharmaceutical Chemistry, Faculty of Pharmacy, Future University in Egypt, Cairo, 11835, Egypt*

[c]*Biomedical Sciences Program, Zewail City of Science and Technology, Giza, 12578, Egypt*

[d]*Department of Pharmaceutics and Industrial Pharmacy, Faculty of Pharmacy, Cairo University, Kasr El-Aini Street, 11562 Cairo, Egypt*

[e]*Department of Pharmacology and Toxicology and Biochemistry, Faculty of Pharmacy, Future University in Egypt, Cairo, 11835, Egypt*

[f]*Institute of Global Health and Human Ecology, School of Sciences & Engineering, The American University in Cairo, AUC Avenue, P.O. Box 74, New Cairo 11835, Egypt*

[g]*King Khalid University, Faculty of Science, Biology Department, Abha 9004, Saudi Arabia*

[h]*Department of Pharmacognosy, Faculty of Pharmacy, El Saleheya El Gadida University, El Saleheya El Gadida, Sharkia, 44813, Egypt*

[i]*Department of Chemistry, School of Life and Medical Sciences, University of Hertfordshire Hosted by Global Academic Foundation, R5 New Garden City, New Capital, Cairo 11835, Egypt. E-mail: sheriffahmy@aucegypt.edu; Tel: +20 1222613344*

† Electronic supplementary information (ESI) available. See DOI: https://doi.org/10.1039/d3ra08779d

‡ Nada K. Sedky and Iten M. Fawzy contributed equally to this work (first co-authors).

strategies are used to treat tumors and limit their progression; surgical resection (especially in early stages), chemotherapeutic agents, and radiotherapy. Both radiotherapy and chemotherapies lack selectivity to cancer cells in addition to possessing high systematic toxicity.[4]

Carboplatin (Cr), a platinum-based drug analog widely used in cancer treatment, can cause tumor cell apoptosis *via* creating DNA damage. It is activated inside the cell, causing G2 phase cell cycle arrest by damaging cell DNA molecules *via* intra- and inter-strand cross-linkage.[5] Cr has broad antitumor activity against head and neck cancer cell lines (SCC61, SQ20B and HEP2).[6] It was also tested against ovarian cancer cell lines (A2780 and OVCAR-3) *in vitro* and *in vivo* and showed significant cancer-killing activities.[7] Cr is also active in non-small cell lung cancer (NSCLC), with an overall response rate of just under 10%.[8] It was also tested against Swiss albino mice with DMH-induced colon hyperplasia, where they reduced the histologic hyperplasia score, upregulated PI3K/AKT/JNK phosphorylation, and elevated caspase 3 levels inducing apoptosis.[9] However, its clinical use is accompanied by several systemic side effects and cancer cells resistance. Thus, several studies have been reported on the nanoformulation of Cr in an attempt to improve its pharmacokinetics properties and pharmacological activity while minimizing its toxic effects.[10]

Finding a solution for the rapid CRC development and the devastating side effects of the commonly used therapeutic agents became an obligate need. One of the recent strategies used is developing nanoparticles (NPs) for many purposes, like drug delivery, imaging, and diagnosis.[11] Various metallic nanoparticles have been fabricated and tested against colon cancer *in vitro* and *in vivo*. Among the widely used metallic NPs (MNPs) are gold, silver, copper, copper oxide, iron oxide and zinc oxide, which have shown promising effects against colon cancer.[12]

Metallic NPs, including copper oxide (CuO) NPs have gained significant attention in nanotechnology and nanomedicine due to their various applications, especially as anticancer agents. CuO NPs showed high cytotoxic effects against HT-29 and HCT-116 cell lines with IC_{50} of 50 and 25 μg mL^{-1}, respectively.[13,14] Nanocomposites formed by loading FDA-approved drugs to metallic NPs have recently been used for targeting therapies for CRC. For instance, 5-fluorouracil (5-FU) was efficiently delivered to CT-26 murine colon.[15–17] Gold NPs were used for loading light-sensitive photosensitizer drugs, which showed a higher effect on the HT-29 colon cancer cell line.[18] Another study reported the anticancer activity of chitin/copper nanocomposite (CNP/CuNP) against MCF-7 breast cancer cells.[19] Indoleamine 2,3-dioxygenase-1 inhibitors (1-MT) loaded copper(I) phosphide nanocomposites (Cu3P/1-MT NPs) induced immunogenic tumor cell death effect by activating CD8+ T cells.[20]

Three general methods are used for the synthesis of CuO NPs; chemical synthesis (sol–gel, co-precipitation and sonochemical methods), physical synthesis (bar milling, microwave assisted and laser ablation) and green synthesis (plant, microorganisms, fungi and algae-based methods).[21,22] The biosynthesis of CuO (green synthesis) using plant extracts has gained attention due to its eco-friendly nature, safety, cost-effectiveness, and high cytotoxic effect on different cancer cells. For instance, the leaf extract of *Pterolobium hexapetalum* was used in the biosynthesis of CuO NPs, showing high cytotoxic activities against MDA-MB-231 breast cancer cells with a high safety margin (where its effect on the cancer cells was more than 1.5 fold more than that of normal ones).[23] Also, another study reported the antiproliferative effect of CuO NPs, synthesized using spinach leaf extract, against MCF-7 cells with IC_{50} value of 21 ± 6 g mL^{-1}.[24] Biogenic synthesis of CuO NPs utilizing fresh leaves of *Ormocarpum cochinchinense* was shown to be effective against colon cancer (HCT-116) with reported IC_{50} of 40 μg mL^{-1}.[25]

Boswellia carterri extracts were revealed to have anti-inflammatory, antioxidant, and antitumor activities.[26] Boswellic acids have been shown to induce apoptosis in colon cancer cells (HT29 cells) *via* inhibition of PI3K/Akt pathway[27] Suhail *et al.* reported that Boswellia essential oil induces apoptosis and suppresses tumor aggressiveness in breast cancer cells (ERpositive T47D cells, human breast cancer MCF7 cells, MDA-MB-231 E1A-transfected breast cancer cells).[28] Boswellia essential oil also decreased β-catenin signaling molecules, suppressing colon cancer stem cell proliferation.[29] In addition to its reported anticancer activity, some studies have shown that some BO components can act as reducing, capping, and stabilizing agents and inhibit the aggregation and agglomeration of the MNPs.[30,31]

In this study, we extracted *Boswellia carterri* essential oil (BCO), using an eco-friendly approach, which was then used as a reducing and capping agent, supporting the biosynthesis of CuO NPs *via* a microwave-assisted approach. Then, Cr was loaded on the greenly synthesized CuO NPs (Cr@CuO), and its Entrapment Efficiency percent (EE%) and release rate were investigated. The obtained NPs were analyzed using ZP, UV-vis, FTIR, X-ray diffraction, and TEM and tested against HCT-116 colon cancer cells. Its efficacy was tested *via* cell viability, apoptosis, and cell cycle analysis assays. Also, computational analysis was carried out to predict Cr and copper oxide interactions. Finally, molecular docking was applied for Cr, CuO, and our prepared CuO–Cr mixture on human alanine aminotransferase 2 to investigate their mechanism of anticancer activity.

Materials and methods

Materials

Copper acetate monohydrate and carboplatin were purchased from Sigma Aldrich, Germany. Dulbecco's Modified Eagle Medium (DMEM) and fetal bovine serum (FBS) were obtained from Gibco (Thermoscientific, Germany). Phosphate-buffered saline (PBS, pH 7.4) was obtained from Lonza Bioscience (Walkersville, USA). Penicillin–streptomycin mixture was attained from Lonza (Bioscience, Switzerland). Annexin V-FITC apoptosis detection kit was purchased from Abcam Inc. (Cambridge Science Park, Cambridge, UK). Propidium iodide was obtained from Calbiochem (Darmstadt, Germany). The remaining reagents were all of analytical grade.

Boswellia carterii essential oil extraction

100 g of fresh *Bosweilla carterii oleogum resins* were hydro-distilled using Clevenger-apparatus for 90 min to extract the essential oil as described by Elyemni *et al.*[32]

GC-MS analysis

Boswellia carterii essential oil extract was analyzed with gas chromatography (GC) (7890B), equipped with Agilent 19091S-433 UI, HP-5MS UI column (30 m × 0.25 mm internal diameter and 0.25 μm film thickness), and mass spectrometer detector (MS) (5977B). Helium was chosen to be the carrier gas, flowing with a rate of 1.0 mL min^{-1} and at a split ratio of 30 : 1. A volume of 1 μL of *Boswellia carterii* essential oil extract was injected, and the temperature program was set to 40 °C for 1 min then it raised to 150 °C with a rate of 4 °C min^{-1} and held for 6 min. Then, temperature was raised again to reach 210 °C with a rising rate of 4 °C min^{-1} and held for another 1 min. Finally, temperatures of 280 °C and 220 °C were set for the injector and detector, respectively. For MS, 70 eV was set for electron ionization (EI) with *m*/*z* ranging between 50 and 450 and 6 min for solvent delay. And finally, the sample was run for 50.5 min to identify the extracted oil constituents. Wiley and NIST Mass Spectral Library data was used to identify the sample's constituents *via* comparing the obtained spectrum fragmentation pattern.[33,34]

Microwave-assisted green synthesis of CuO nanoparticles

CuO NPs were greenly synthesized *via* a microwave-assisted approach using *Boswellia carterii* Essential Oil (BCO) and copper acetate monohydrate according to the previously reported with few modifications.[35] The oil acts as a reducing and capping agent, supporting nanoparticle preparation. In brief, BCO and copper acetate monohydrate (1 : 10) were added to 20 mL of deionized water and stirred. After that, the mixture was transferred to a microwave and heated for a total duration of 5 min (10 cycles of 30 seconds each). The obtained metal hydroxide paste was then calcined at 600 °C for 5 hours to obtain the desired metal oxide nanoparticles that were used for further characterization.[36]

Preparation of Cr/CuO NPs (Cr@CuO NPs)

A specific amount of the prepared CuO NPs was added to 15 mL of deionized water and stirred for 15 min. After that, an aqueous solution containing Cr was added dropwise to CuO NPs and kept on a magnetic stirrer at RT for 24 h. Then, the formed solution was sonicated for 15 min, centrifuged (12 000 rpm, 1 h), dialyzed against deionized water for 24 h, and lyophilized.

Physicochemical characterization of the prepared nanoparticles

Zeta potential analysis. Zetasizer Nano ZS (Malvern Instruments, Herrenberg, Germany) was used to measure the zeta potential of the prepared CuO NPs by dispersing a small amount of the metal oxide NPs in distilled water. The refractive index was set to 1.33, and water viscosity was 0.887 mPa s. Consequently, the dispersion was sonicated for 5 minutes in a SONOREX DIGITAL 10 P bath sonicator (BANDELIN electronic GmbH & Co. KG, Berlin, Germany). HeNe laser (10 mW) was used with a wavelength of 633 nm and the measurements were detected with a backscatter angle of 173°. The measurement was carried out utilizing laser doppler velocimetry (Malvern Instruments, Herrenberg, Germany) at room temperature (~25 °C).

Fourier-transform infrared spectroscopy (FTIR). Infrared absorption spectra of the synthesized nanoparticles were observed using Fourier Transformed Infrared Spectroscopy (FTIR) on a Nicolet 380 spectrometer (ThermoScientific Nicolet, Waltham, MA, USA). For FTIR studies, the metal oxide nanoparticles were mixed with potassium bromide. The measurement was carried out in the transmittance mode at a frequency range of 4000–400 cm^{-1}.[37]

X-ray diffraction analysis (XRD). XRD patterns of the metal oxide NPs were obtained using (Bruker D8 Discover X-ray diffractometer), with an IV diffractometer operating at 40 kV, 40 mA, and a CuKα radiation wavelength of $\lambda = 1.5406$ Å. The 2 theta scale ranged from 10 to 80° with a 0.02° step size for phase identification. The average particle diameter (*D*) was calculated for the NPs, using the obtained diffractograms. The calculations were performed using the Debye–Scherer's eqn (1);

$$D = \frac{k\lambda}{\beta \cos \theta} \quad (1)$$

where *k* (0.9) is the shape factor, lambda is the X-ray wavelength of Cu K radiation 1.54 Å, theta is the Bragg diffraction angle, and beta is the full width at half maximum (FWHM) of the respective diffraction peak.[38]

High-resolution transmission electron microscopy (HRTEM). High-resolution transmission electron microscopy (TEM) (JEOL-JEM 2100) (Musashino, Akishima, Tokyo, Japan) was used for characterizing the prepared nanoparticles' vis-à-vis their morphology. The NPs' diameters were measured using ImageJ's image processing software (NIH, Bethesda, MD, USA).[39] Also, the same software was used to measure the interplanar distance of the CuO lattice fringes. The selected area electron diffraction (SAED) pattern was found using transmitted and one of the diffracted beams.

Determination of entrapment efficiency percent (EE%) of Cr in Cr@CuO NPs. The EE% of Cr EE% in Cr@CuO NPs was determined as previously with slight modifications.[40,41] 2 mL of the prepared Cr@CuO NPs was centrifuged (15 000 rpm, 2 h, 4 °C); (Hermle Z 326 K, Labortechnik GmbH, Wehingen, Germany). Then, the supernatant was ultrafiltrated, and the unencapsulated Cr was quantified using HPLC, as described in the ESI.† The EE (%) of Cr@CuO NPs was determined using eqn (2).[42]

$$\text{EE\%} = \frac{\text{total amount of drug} - \text{the amount of drug unencapsulated}}{\text{total amount of drug}} \times 100 \quad (2)$$

Release study. Dialysis membrane technique was used to investigate the Cr release rate from Cr@CuO NPs using a dialysis bag (12–14 kD cut off). In brief, 0.5 mL of Cr@CuO NPs was loaded into a dialysis bag, placed into a vessel containing 25 mL of PBS (pH value of 5.5), and shaken in a shaking incubator at 37 ± 0.5 °C. HPLC (described in ESI†) was used to quantify the sample by collecting 1 mL at certain time intervals and replacing it with 1 mL of warmed buffer. These measurements were repeated in triplicates and standard deviations were computed.

Biological assays

Cell culture. Both HCT-116 and CCD 841 CoN cells were brought from the ATCC. The cells were seeded in culture plates with DMEM media and placed in a 5% CO_2 humidified incubator where the temperature was adjusted to 37 °C. When the cells reached 70% confluency, the culture media was replaced by a fresh one.

Cytotoxicity screening. A suspension of HCT-116 and CCD 841 CoN cells in complete culture media was added to the 96-well plates at a concentration of 5000 cells per well. After 48 h of incubation with the media containing various concentrations of Cr, CuO NPs, and Cr@CuO NPs, cellular proliferation of both cells was evaluated using SRB assay as demonstrated in our previous work.[43] Simply, cells were first exposed to a fixation step by removing the culture media and adding 150 μL of 10% TCA instead. The cells were left together with the TCA for 1 h at 4 °C. The TCA solution was then discarded, and cells were subjected to washing with distilled water for 5 consecutive rounds before being incubated with SRB solution in a dark room for 10 min. Thereafter, cells were exposed to 3 rounds of was with 1% acetic acid, left to dry overnight and 150 μL of TRIS (10 mM) was put in each well to dissolve the stain. At last, absorbance was detected at 540 nm using a BMGLABTECH®-FLUOstar Omega microplate reader (Ortenberg, Germany).

Apoptosis. Apoptosis analysis was carried out using Annexin V-FITC apoptosis detection kit (Abcam Inc., Cambridge Science Park, UK). HCT-116 cells were cultured as described in the cytotoxicity assay. After 48 h of incubation with Cr (8.24 μg mL^{-1}), CuO NPs (11.25 μg mL^{-1}), and Cr@CuO NPs (5.17 μg mL^{-1}), cells were detached using trypsin, harvested, washed with ice-cold PBS twice, and resuspended in 500 μL of Annexin V-FITC/PI solution in a dark place. Thirty minutes post-incubation, cells were injected ACEA Novocyte™ flowcytometer (ACEA Biosciences Inc., SanDiego, CA, USA) which was coupled with two fluorescent channels for detecting FITC and PI signals. Apoptosis detection by quadrant analysis was performed using ACEA NovoExpress™ software.

Cell cycle. Forty-eight hours post-incubation with the test agents, HCT-116 cells were evaluated for cell cycle kinetics using the PI staining method.[44] An estimate of 10^5 cells were detached using trypsin, washed with ice-cold PBS (pH 7.4), and fixed by placing in 2 mL of 60% cold ethanol for 1 h at 4 °C. This was followed by a second round of washing with PBS before resuspending the cells in the buffer containing 50 μg mL^{-1} RNAase A and 10 μg mL^{-1} PI for staining at room temperature in the dark atmosphere for 20 min. Lastly, cells were transferred to Novocyte™ flow cytometer to carry out the cell cycle analysis and compute the percentage of cell population at each cell cycle stage.

RT-qPCR. RNA extraction was done using QIA amp Viral RNA Mini Kit (Qiagen, Hilden, Germany) as per the manufacturer's guidelines. The concentration of the isolated RNA was determined using Nanodrop Spectrophotometer at A260/280 ratio. Then, the process of cDNA synthesis was carried out using the ReverAid RT Kit (ThermoFisher Scientific, Waltham, USA) as prescribed in our previous work,[43] and the reaction components are provided in the ESI (Table S1†). Finally, RT-qPCR assay was run for the target genes (Bax, Bcl-2, and p53), as well as the housekeeping gene (β-actin) using the Qiagen Quanti Nova SYBR Green PCR Kit (cat # 208052), the primers presented in Table S2,† and the reaction components in Table S3.† The reactions were operated on Rotor-Gene Q-Qiagen Real-time PCR thermal cycler, and the $2^{-\Delta\Delta C}{}_t$ method was implemented to calculate the relative normalized gene expression as described.[43]

Computational methods

First, the interaction type between Cr and copper oxide was assessed using Discovery Studio 4.1. Cr structure was downloaded from PUBCHEM in a readable extension and copper oxide was built up using the drawing tools of Discovery Studio. Both Cr and copper oxide were subjected to minimization using CHARMM forcefield and Momany-Rone to render metals in a readable energy.

Then, Cr was identified as a receiver molecule and copper oxide as a ligand. The favorable charge and molecule percentage were calculated *via* energy minimization simulation studies and analysis of ligand poses after the interaction.

Later, human alanine aminotransferase 2 was downloaded from PDB with code: 3IHJ. The enzyme was cleaned for missing residues and minimized, applying the same forcefield. Then, the protein was defined as a receptor, and the C-docker protocol was adopted for molecular docking studies between aminotransferase and complexed ligand, copper oxide, Cr alone, and the mixture of Cr and copper oxide. Furthermore, Ramachandran Plot was generated to verify predicted torsion angles in protein during interaction with the mixture.

Statistical analysis

Statistical analysis of the results was performed using SPSS 20.0, while the graphical representations were all plotted with GraphPad Prism 6.0. The data are displayed as the mean ± standard deviation (SD) throughout the study. Statistical analysis was considered at *P*-values less than 0.05. One-way analysis of variance (ANOVA) with multiple comparisons was used for normally distributed data.

Results and discussion

BCO GC-MS chemical composition analysis

Several peaks for essential oil extract were detected *via* GC-MS chromatogram analysis, as shown in Fig. 1. The obtained MS was compared to the NIST library to identify essential oil

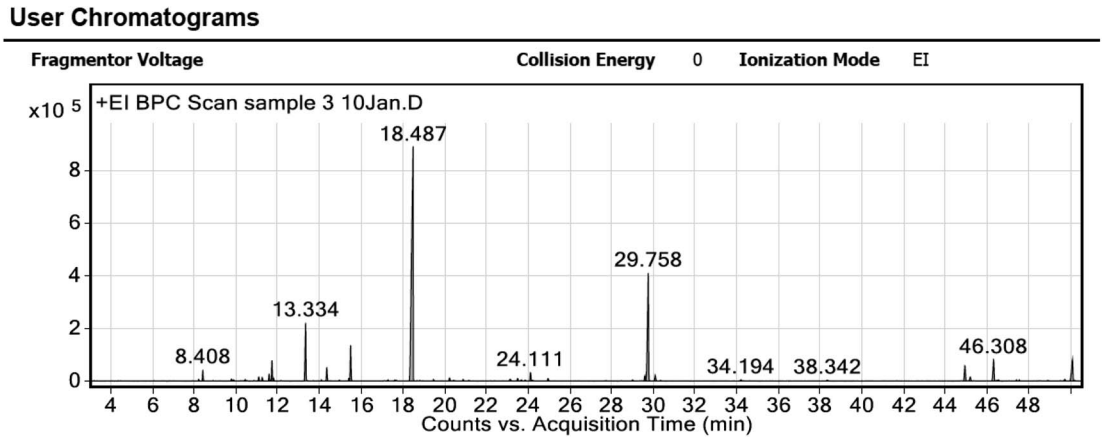

Fig. 1 The GC-MS chromatogram of volatile oil extracted.

constituents, as listed in Table 1. The most abundant component was *trans*-nerolidol (16.41%), and the second was verticiol (3.04%) followed by DL-limonene and linalool (1.98% and 1.31%, respectively) as major components; the mass spectra of these components were illustrated in Fig. S1a–d,† respectively.

Physicochemical characterization of the prepared nanoparticles

Zeta potential (ZP) analysis. Zeta potential analysis, a measurement of NPs' surface charges, was used to investigate the relative stability of the greenly synthesized CuO NPs prepared *via* microwave methods. High ZP values indicate high stability with a low aggregation potential due to their repulsive tendency to each other.[45] Our findings showed ZP of −24.6 mV, which is consistent with the previous finding of similar CuO NPs prepared by algal-mediated synthesis and *Murrya koenigi* water extract-mediated synthesis, revealing similar negative charges of the nanoparticles.[46,47] On the other hand, the Cr@CuO NPs showed a ZP of −13.6 mV, revealing a lower negative charge after Cr entrapment. The reduction in negative charge is attributed to the loading of the positively charged Cr (resulting from the platinum drug's initial aquation reaction where the chloride groups are switched with the water molecules).[48]

Fourier-transform infrared spectroscopy (FTIR). FTIR spectra of *B. carterii* oil extract, CuO NPs, Cr, and Cr@CuO are presented in Fig. 2. FTIR spectrum of BO shows sharp peaks at 3464, 2916, 1741, 1456, 1365, 1238 and 1050 cm^{-1}, which correspond to alcohol, carboxylic acid, ester, alkene, alkane and

Table 1 Chemical composition of volatile oil extracted

Peak	RT	Compound	Area sum (%)
1	8.208	α-Fellandrene	0.12
2	8.408	α-PINENE	0.96
3	9.777	Sabinene	0.17
4	9.861	2-β-PINENE	0.14
5	10.433	β-Myrcene	0.13
6	11.583	*p*-Cymene	0.66
7	11.723	DL-Limonene	1.98
8	11.797	Eucalyptol	0.24
9	13.334	Formic acid, octyl ester(octyl formate)	6.35
10	14.348	Linalool	1.31
11	17.617	α-Terpineol	0.1
12	18.487	Acetic acid, octyl ester(octyl acetate)	51.83
13	19.465	CARVONE	0.14
14	23.496	Neryl acetate	0.26
15	23.682	*n*-Decanoic acid	0.13
16	23.859	α-Copaene	0.09
17	27.756	9-Decen-1-ol	0.09
18	29.599	Lilac alcohol	0.63
19	29.758	1,6,10-Dodecatrien-3-ol, 3,7,11-trimethyl-, (*E*)-(*trans*-nerolidol)	16.41
20	45.195	Cembrene	0.52
21	46.308	Verticiol	3.04
22	47.411	Thunbergol	0.12

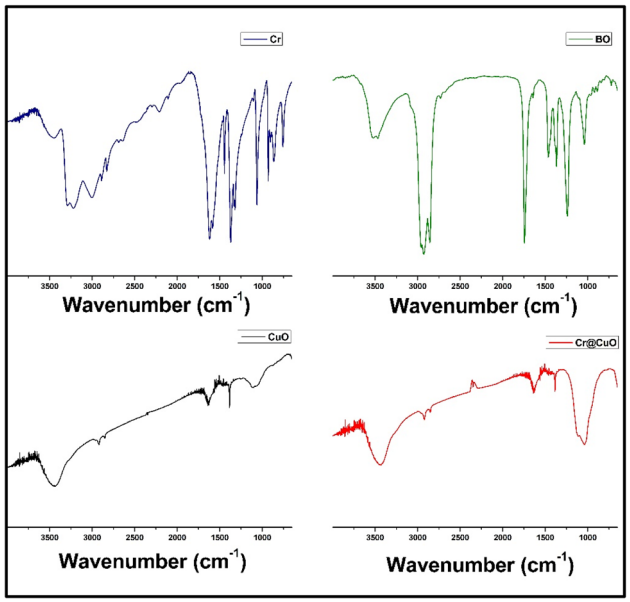

Fig. 2 FTIR spectra of Cr, BO, CuO NPs, and Cr@CuO NPs.

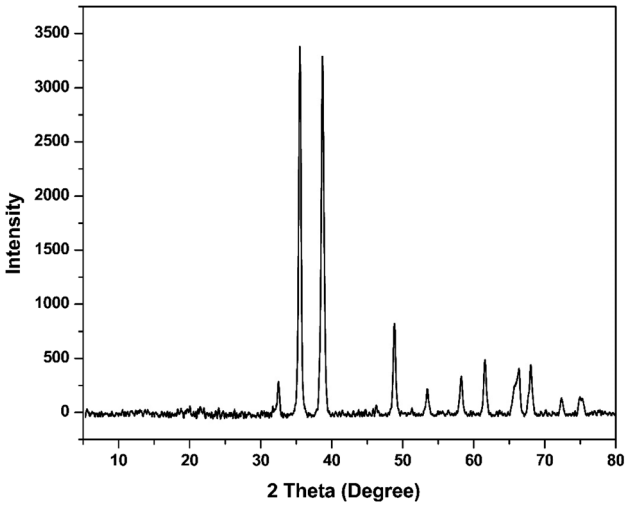

Fig. 3 XRD pattern of CuO NPs.

alkyl amine and alkyl halides functional groups, respectively. They are also consistent with the peaks reported before.[49] FTIR charts of the prepared metal oxide NPs showed absorption peaks at 532 cm^{-1} (strong peak), indicating the formation of CuO where it is assigned to Cu–O bond bending vibration.[50] Other peaks were observed at 3438, 2919, 1630, 1381, and 1112 cm^{-1}, which may be attributed to the remaining BO in the CuO NPs. These peaks are slightly shifted and show very low intensities, indicating that these functional groups may be involved in the reduction process. Cr FTIR shows distinguished peaks at 3201 and 3282 cm^{-1} that may be attributed to the N–H stretching of the primary amine, while the peak found at 2993 cm^{-1} corresponds to the alkane C–H stretching. The NH and NH_2 bending vibrations were observed from the 1612 and 1444 cm^{-1} peaks, respectively. The second characteristic peaks is for Pt–NH_2 bond at 1369 and 1319 cm^{-1}. These 2 conspicuous peaks for the main functional groups in Cr were previously reported.[51] The carbonyl group of carboplatin was presented by the peak found at 1048 cm^{-1}.[52]

Mimicking the peaks in the CuO NPs' chart, Cr@CuO FTIR chart exhibits the same peak at 532 cm^{-1} attributed to Cu–O bond. The peaks indicating the remaining BO are found at 3438, 2919, 1621, 1382, and 1112 cm^{-1}. Similarly, these peaks are slightly shifted and with reduced intensity. In addition, a strong peak was detected at 1048 cm^{-1}, which can be attributed to the loaded Cr carbonyl group.

X-ray diffraction analysis (XRD). XRD pattern of CuO NPs prepared *via* microwave revealed pure CuO NPs in crystalline nature. The present experimental results were found to be identical to that of pure CuO, confirming the successful synthesis of pure CuO NPs.[21,53,54] As previously reported with CuO NPs XRD patterns,[38] 11 main peaks in the diffraction patterns were observed to be at $2\theta = 32.50$, 35.52, 38.72, 48.84, 53.47, 58.24, 61.59, 66.12, 68.02, 72.38, and 75.12° (Fig. 3). All 11 peaks were sharp with no significant broadness. Also, they can be indexed to the monoclinic crystal system CuO (*C*2/*c* space group, JCPDS card no. 45-0937), with no additional impurity peaks, thus, the prepared CuO NPs are highly pure. On the other hand, the nanocrystalline nature of CuO NPs is shown by the sharp structural peaks present in the XRD pattern and the crystallite size found to be 63.15 nm (<100 nm).

Transmission electron microscopy (TEM). Transmission electron microscopy (TEM) analysis was performed to determine the morphology and particle size distribution of CuO NPs. The CuO NPs and the Cr@CuO NPs' morphologies are shown in Fig. 4A and C, respectively. The CuO NPs and the Cr@CuO NPs' diameter distribution histograms (presented in Fig. 4B and D, respectively) were created using NPs' diameters obtained *via* ImageJ (NIH, Bethesda, MD, USA). The average diameters of CuO NPs and the Cr@CuO NPs' were calculated and found to be 119.06 ± 21.49 nm and 135.84 ± 26.88 nm, respectively. The higher average diameter of Cr@CuO NPs' compared to the average CuO NPs' diameter can be justified by the Cr loading to the CuO NPs. The size range of the aggregates was found to be 500–1000 nm, demonstrating the capability of the synthesized NPs to accumulate in the cancer cells *via* passive targeting. Previous studies showed that the nanoparticles' size, even in aggregation into hundreds of nanometers (50–2000 nm) can accumulate in solid tumors due to their leaky vasculature.[55,56]

In addition, the interplanar distance between CuO NPs' lattice fringes was found to be 0.29 nm, which is in harmony with previously reported studies,[57] confirming the CuO NPs' formation. The magnified lattice fringes of CuO NPs are displayed in Fig. 5A. On the other hand, as shown in Fig. 5B, the selected area electron diffraction (SAED) pattern of CuO NPs presented diffraction patterns involving sharp spots; hence, the structures of these NPs must be ordered.[38]

Entrapment efficiency percent (EE%) and *in vitro* release assay. The EE% of the Cr in the Cr@CuO NPs was found to be 78.9 ± 5.9%. The high EE% of the Cr@CuO NPs can be justified by the adsorption and binding interactions between the

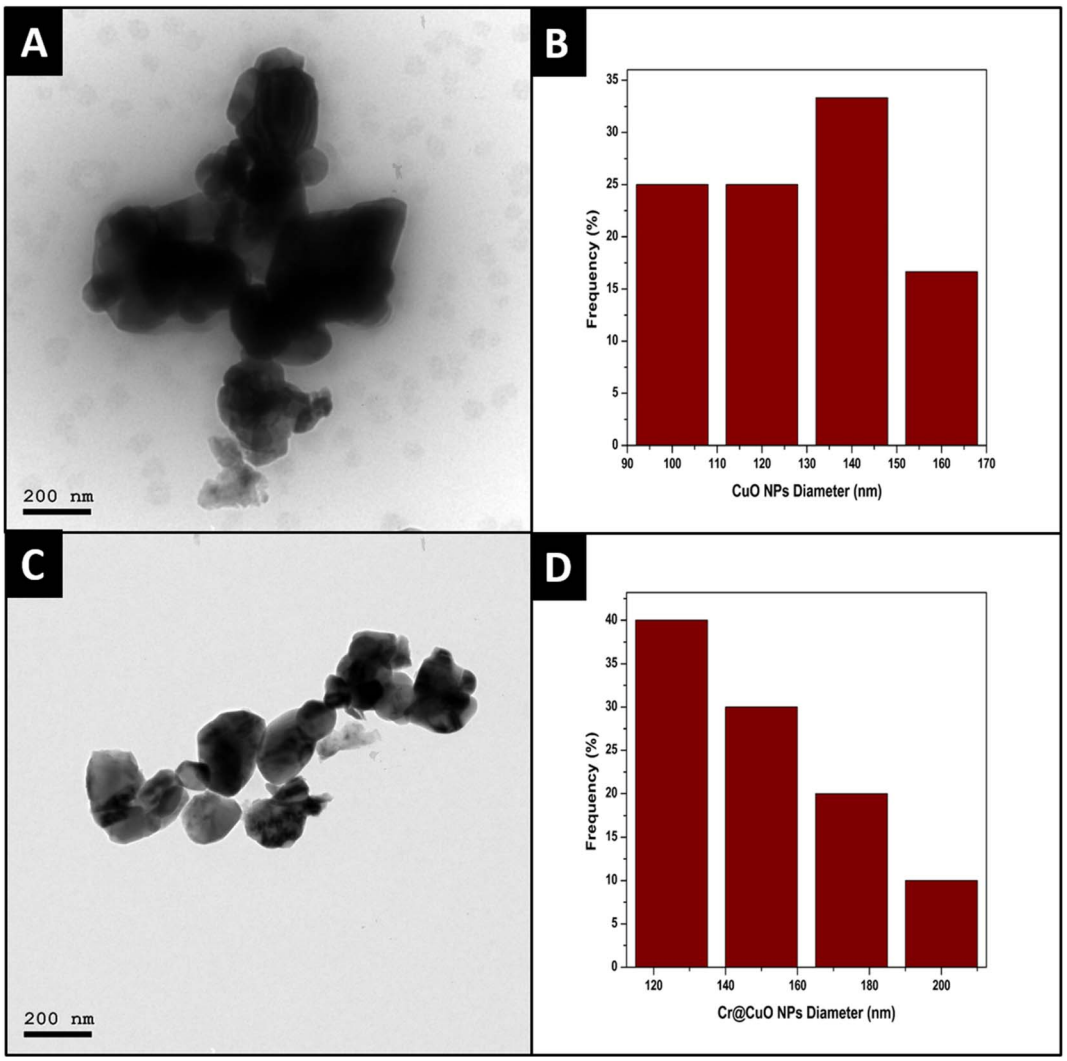

Fig. 4 TEM micrographs of CuO NPs (A) and Cr@CuO NPs (C) and their particle diameter distribution histograms (B and D, respectively).

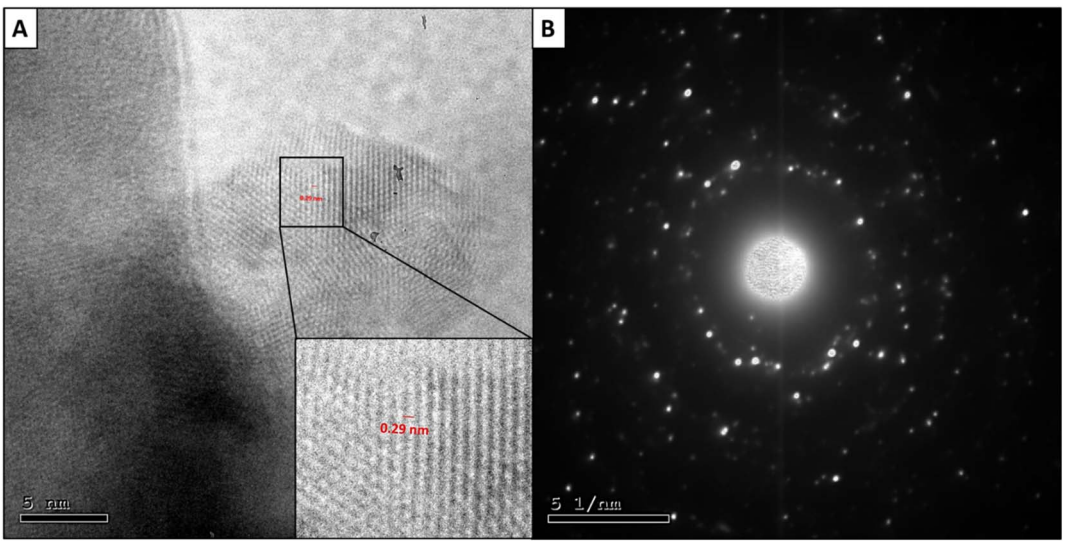

Fig. 5 The magnified lattice fringes (the interplanar distance = 0.29 nm) (A) and SAED pattern (B) of CuO NPs.

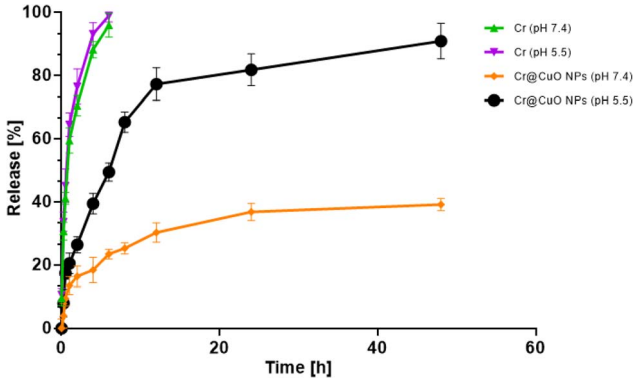

Fig. 6 The release profiles of unloaded Cr and Cr@CuO NPs at pH 5.5 and pH 7.4.

negative charges on the surface of CuO NPs and the positively charged Cr molecules. of ionic attraction of the positively charged Cr into the negatively charged CuO NPs. Thus, electrostatic interaction plays an essential role in such a high EE%.[58]

To determine the appropriateness of CuO NPs as chemotherapeutic carriers, *in vitro* release study of Cr from Cr@CuO NPs, utilizing two dissimilar pH media mimicking the tumor microenvironment (pH 5.4) and the physiological conditions (pH 7.4), was carried out and compared to the free Cr. The release of Cr from Cr@CuO NPs was pH-dependent (Fig. 6). At pH 5.5, a triphasic release behavior was observed for the release of Cr from the Cr@CuO NPs over the 48 h-duration of the release test. Different release mechanisms controlled each of the three phases: dissolution, diffusion, and erosion.[59] In the first 2 h, rapid release of Cr was detected (26.42%), which is linked to the Cr molecules present on the CuO NPs' surface. The partition of Cr to be dissolved in water was encouraged by the solubility of Cr in water.[60] The small particle size supports the large surface area of the CuO NPs. At this stage, the Cr is only challenged by the dissolution mechanism to be soluble and released in the medium. The next phase extended until 12 h of the release test, where 77.30% was released in the medium. At the second stage, the entrapped Cr in the outer layer of the CuO NPs matrix dissolves and diffuses to reach the release medium. Hence, the second phase is limited by both the drug's dissolution and diffusion to be released from the nanoparticle matrix. The last phase presents the slowest Cr release rate, reaching 90.92% of a cumulative released drug after 48 h since the beginning of the *in vitro* release assay. This phase is the slowest since it is controlled by an additional mechanism (erosion) besides the previously mentioned mechanisms (dissolution and diffusion). The erosion is added to the release challenges since the drug in the innermost core of the nanoparticle will have to travel a long distance in the CuO NP matrix before reaching the interphase between the medium and the matrix. Cr@CuO NPs showed a sustained release profile in comparison to the free Cr release profile in which 98.95 ± 2.00% of the Cr was released in the first 6 h of the release test. The sustained release of Cr for a prolonged period was tuned by the particle size of CuO NPs.[61]

In contrast, at physiological conditions (pH 7.4) the release rates of Cr from Cr@CuO NPs at pH 7.4 were much slower as compared to those observed at (pH 5.5). The release rates were 16.5%, 30.3% and 39% at 2 h, 12 h and 48 h, respectively. The higher percentage of drug release in the acidic medium might be attributed to the release of copper ions (Cu^{2+}) in the acidic medium[62] and the protonation of Cr, subsequently strengthening the repulsive forces leading to faster release of rates of Cr, as compared to that at physiological pH.[63] A triggered pH-dependent behavior is beneficial in cancer therapy. At pH 7.4 (mimicking physiological conditions), it is anticipated that most of the loaded drug will remain adsorbed to the surface of metallic NPs, with no high release and thus providing stability when found in the plasma, with minimum toxic effects on the normal tissues. Thereafter, the drug will rapidly be released when the NPs reach the cancer cells (pH 4.5–6) tumor cells, which will definitely augment the efficacy of the preferential cancer therapy.[64]

Biological assays

Cytotoxicity screening. Cr is a broad-spectrum platinum drug that is commonly used as an anticancer agent against colorectal carcinoma. However, its use still faces some limitations, including but not limited to systemic side effects and the emergence of drug resistance.[10] It is worth mentioning that CuO NPs have previously demonstrated potent antitumor activity against HCT-116 colon cancer cells.[25] In this context, the current study is focused on introducing Cr onto CuO NPs as a promising drug delivery system (Cr@CuO NPs) to HCT-116 cancer cells to improve its therapeutic efficacy and reduce its systemic side effects. The antiproliferative effects of Cr, CuO NPs, and Cr@CuO NPs were determined against both human HCT-116 cancer and CCD 841 CoN normal cell lines using SRB assay. The IC_{50} values were computed using a logarithmic scale of ten different concentrations ranging from 0.01 to 300 μg mL^{-1} for each investigated agent. The dose–response curves are clearly presented in Fig. 7A–C. Numerous studies calculated the selectivity index (SI) as a direct ratio of IC_{50} values derived for healthy and malignant cells.[65–67] This study calculated the SI of all the investigated agents to show their safety profiles. The observed results are recorded in Table 2.

The IC_{50} of Cr and CuO NPs were estimated to be 8.24 μg mL^{-1} and 11.25 μg mL^{-1} on HCT-116 cancer cells as shown in Table 2 and Fig. 7A, B. Meanwhile, Cr@CuO NPs exhibited the highest antiproliferative activity against HCT-116 cells with an IC_{50} of 5.17 μg mL^{-1} which was 1.6 and 2.2 folds higher than that of Cr and CuO NPs treated groups, Table 2 and Fig. 7C. Therefore, loading Cr onto the greenly synthesized CuO NPs proved to be a successful approach for improving the efficacy of Cr where CuO NPs exerted a synergistic effect and potentiated the actions of Cr. Our drug (Cr) has usually been limited by its poor cellular uptake and the demand for high therapeutic doses. *In vitro* studies showed that the incorporation of Cr in nanoparticles could be a valuable approach to enhance its delivery and reduce the required dose.[68] In the modern era, copper nanoparticles have become a rising bio-nanotechnology approach in cancer therapy.

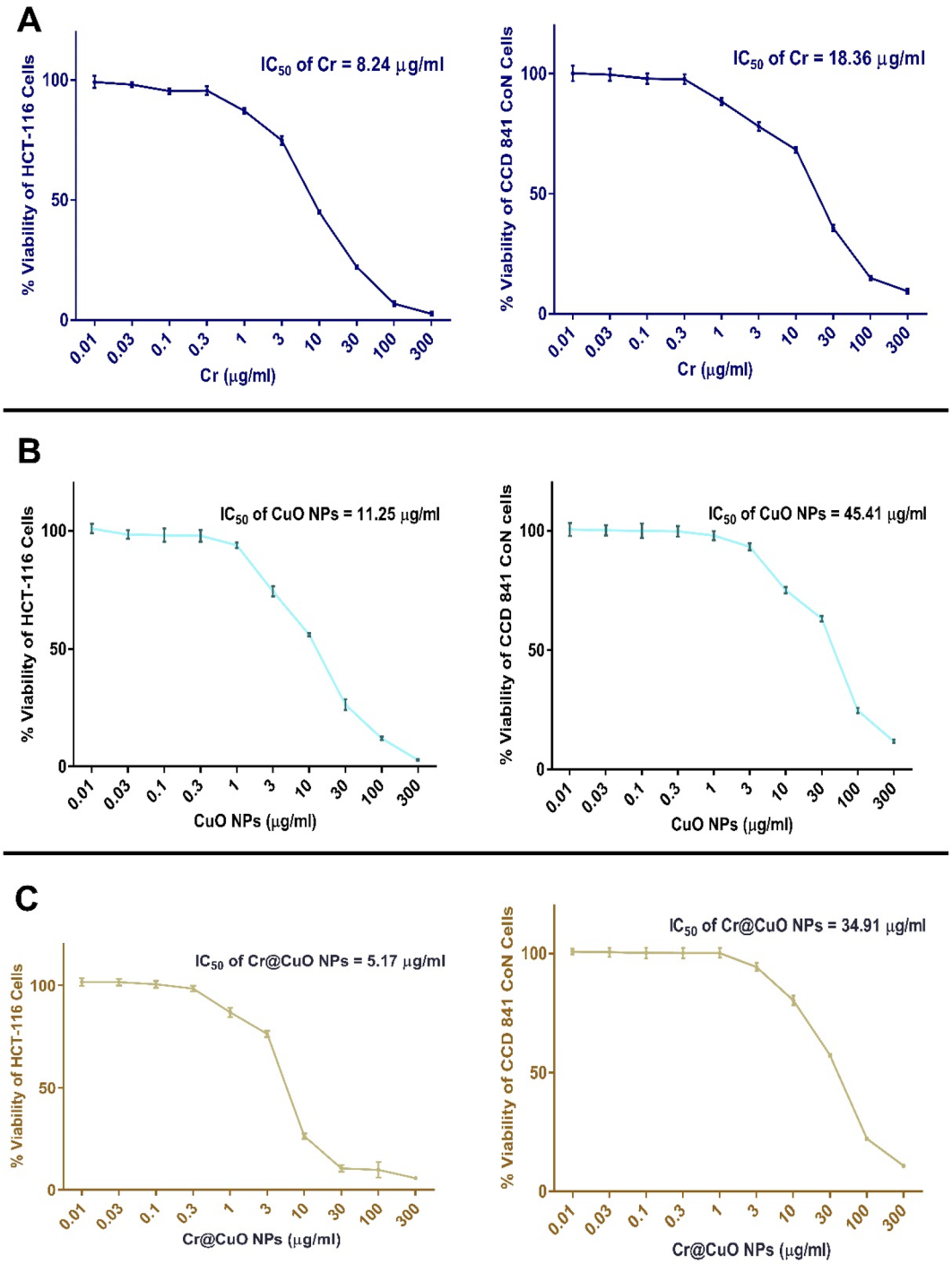

Fig. 7 Dose–response curves display the percentage viability of HCT-116 (left panel) and CCD 841 CoN cells (right panel) after 48 h of exposure to Cr (A), CuO NPs (B), and Cr@CuO NPs (C), respectively.

Such NPs are believed to function as DNA-cleaving and powerful anticancer agents, which could be attributed to their capacity for binding, ability to modify their surface properties through conjugation with other chemotherapeutics, effectiveness as a nano-drug delivery system with much affordable costs than that of Ag or Au, and their ability to act as molecular doping operators that could manipulate the cell cycle.[69]

The SI values for pure Cr and CuO NPs were 2.23 and 4.04, respectively. Interestingly, Cr@CuO NPs attained the highest SI (SI = 6.82) towards cancer cells and achieved the uttermost safety profile among all other treatments, Table 2. The loading of Cr onto Cr@CuO NPs improved its selectivity by 3-times compared to the pure Cr treatment. A Similar approach was performed previously where Cr together with doxorubicin (Dox) were dual loaded onto ZnO nanoparticles and proved highly

Table 2 Cytotoxicity against human colon cancer (HCT-116) and normal colon epithelial (CCD 841 CoN) cells following exposure to the test agents for 48 h[a]

Test agent	IC_{50} on HCT-116 cells (μg mL^{-1})	CC_{50} on CCD 841 CoN cells (μg mL^{-1})	SI (CC_{50}/IC_{50})
Carboplatin (Cr)	8.24 ± 0.74	18.36 ± 1.12	2.23
Copper oxide NPs (CuO NPs)	11.25 ± 1.04	45.41 ± 2.16	4.04
Copper oxide NPs loaded carboplatin (Cr@CuO NPs)	5.17 ± 0.48	34.91 ± 1.08	6.82

[a] Data presented as the mean IC_{50} of three trials ± standard deviation (SD).

efficient at increasing the sensitivity and selectivity of chemo drugs to human breast adenocarcinoma cells.[70]

All the above reinforces the idea that our newly synthesized Cr@CuO NPs possess much better therapeutic potential than free Cr or CuO Nps in the treatment of colon cancer.

Apoptosis. SRB assay showed that incorporating Cr into CuO NPs induced a significant improvement in its antiproliferative effects against HCT-116 cancer cells. Nevertheless, additional experiments such as apoptosis assay and flow cytometric analysis were performed to reveal the mechanism of cell death in HCT-116 following incubation with Cr, CuO NPs, and Cr@CuO NPs at their estimated IC_{50} concentrations for 48 h. Untreated HCT-116 cells were utilized as the control group. The obtained results are recorded in Table 3 and Fig. 8. The percentage of the cellular population undergoing early apoptosis was not affected much with CuO NPs treatment but increased significantly upon exposure to Cr treatment (P-value ≤ 0.05). The Cr@CuO NPs treatment induced a remarkable elevation in the cellular population of the early apoptosis quartile, which even exceeded that with Cr treatment by 5.4-folds (P-value ≤ 0.001). Regarding the late apoptosis quartile, a significant elevation in the cellular population was observed amongst all treatment groups as compared to control (untreated) cells. Interestingly, Cr@Cuo NPs caused a remarkable increase in the cellular population undergoing late apoptosis by 4.6 and 6.4 folds when compared with Cr ($P \leq 0.001$) and CuO NPs ($P \leq 0.001$), respectively.

The apoptotic effects of Cr were previously noted on a few cancer cell lines, including non-small cell lung cancer (A549),[71] ovarian (OVCA429),[72] and cervical (SiHa)[73] cancers. The literature search also revealed considerable apoptotic effects for CuO NPs on breast (MCF-7),[74] colorectal (HCT-116),[13] and cervical (HeLa)[75] cancer cells. Therefore, our apoptosis assay findings were in line with the other studies where both Cr and CuO NPs exerted significant apoptotic effects, while Cr@CuO NPs exceeded their apoptotic activity. Our results also showed that Cr@CuO NPs caused a significant reduction in the viable cells by 41.5% and 44.65% when set against Cr and CuO NPs ($P \leq 0.001$). Cr@CuO NPs also caused a 5-fold escalation in the necrotic cell population percentage relative to the control ($P \leq 0.05$). As such, our findings confirmed the cytotoxicity assay results and reinforced the ideology of incorporating Cr onto the greenly synthesized CuO NPs.

Cell cycle analysis. The cell cycle kinetics of HCT-116 cancer cells were examined by DNA flow cytometry after being exposed for 48 hours to Cr, CuO NPs, and Cr@CuO NPs treatments at their corresponding IC_{50} concentrations. Table 4 and Fig. 9 display all the collected data. Apoptotic cells are known to have fractional DNA content on a regular basis due to the extraction of fragmented (low molecular weight) DNA during the staining process and the extrusion (blebbing) of apoptotic bodies.[76] So, they contain only a small portion of DNA and are frequently portrayed on the DNA content frequency histograms as "Sub-G1 phase".[76] Our findings showed a meaningful elevation in Sub-G1 cell populations treated with Cr@CuO NPs compared to the control and all other treatment groups (P-value ≤ 0.001). This, in turn, justifies the distinguished apoptotic properties of Cr@CuO NPs, which exceeded by far that of pure Cr or CuO NPs treatments.

In the synthetic phase, also known as the "S phase", the cell produces an exact copy of its genetic material, *i.e.*, the cell duplicates its DNA content.[77] Treatment with Cr, CuO, and Cr@CuO NPs significantly reduced cell population at the S phase compared to the control group (untreated). So, all treatment groups displayed a noticeable activity in decreasing DNA synthesis. It is worth emphasizing that Cr@CuO NPs also surpassed free Cr and CuO NPs at reducing the frequency of cells undergoing DNA duplication ($P \leq 0.001$).

G2 is the pause stage following S phase during which the cell gets ready to enter mitosis (M). CDK1 usually regulates the transition from G2 to M. However, when the brakes go wrong,

Table 3 Apoptosis assay of the HCT-116 cells using annexin/PI stain flow cytometric analysis[a]

Apoptotic stage of HCT-116	Control	Cr (8.24 μg mL^{-1})	Cuo NPs (11.25 μg mL^{-1})	Cr@Cuo NPs (5.17 μg mL^{-1})
Necrosis (Q2-1)	0.52 ± 0.17	2.11 ± 0.22	3.41^{**} ± 1.26	2.56^{*} ± 0.17
Late apoptosis (Q2-2)	1.05 ± 0.24	7.68^{***} ± 0.99	5.61^{**} ± 0.96	$35.66^{***\#\#\#\$\$\$}$ ± 0.23
Viable cells (Q2-3)	97.22 ± 0.24	87.24^{**} ± 1.09	90.41^{**} ± 2.20	$45.76^{***\#\#\#\$\$\$}$ ± 0.92
Early apoptosis (Q2-4)	1.21 ± 0.18	2.97^{*} ± 0.09	0.58 ± 0.18	$16.02^{***\#\#\#\$\$\$}$ ± 1.01

[a] Data presented as mean ± SD. (*), (#) and ($) represent significant differences compared to the Control, Cr and Cuo NPs treated groups, respectively. Statistical analysis was performed using one one-way ANOVA test with Tukey post hoc test.

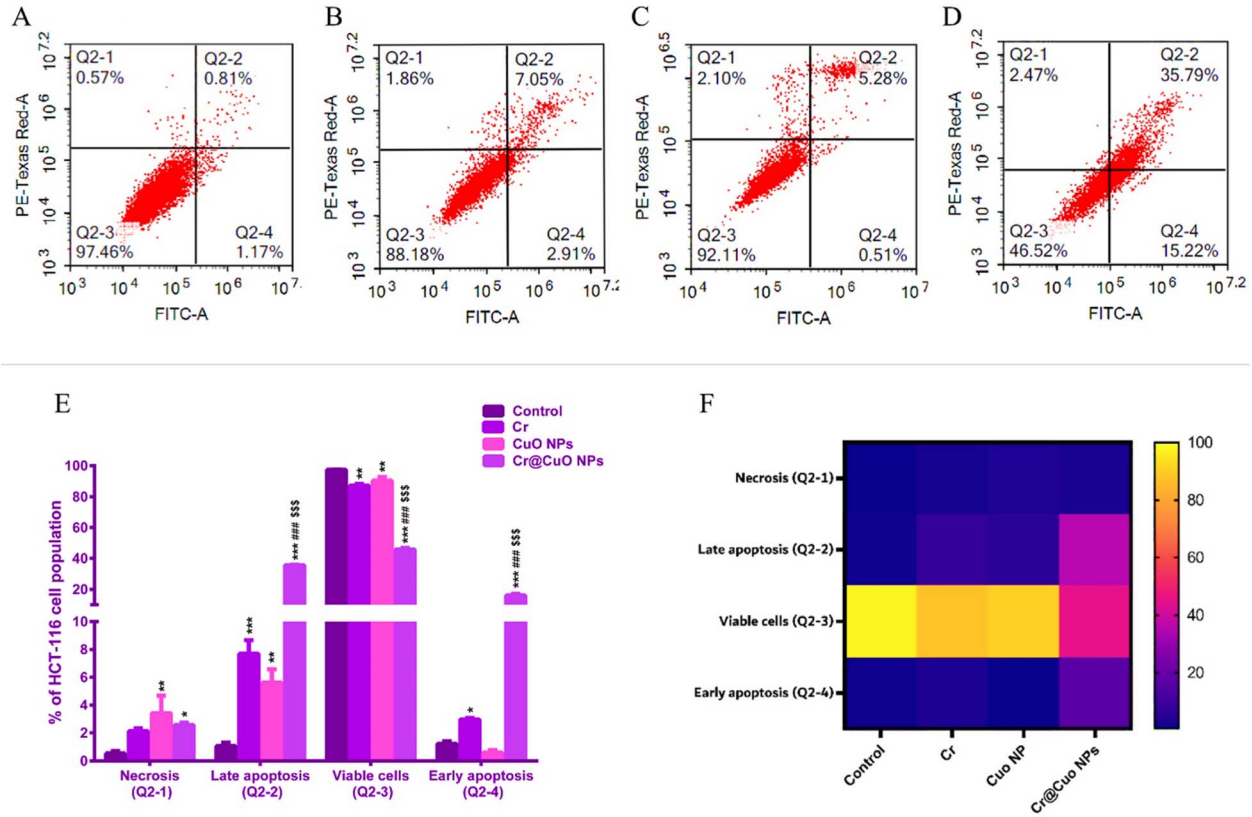

Fig. 8 Cytograms display the annexin V/propidium iodide – staining of the control (untreated) HCT-116 cells (A), and those treated with Cr (B), CuO NPs (C), and Cr@CuO NPs (D) following 2 days of incubation. Quadrant charts (E) show the apoptosis assay results where Q2-1 (necrotic cells, AV-/PI+), Q2-2 (late apoptotic cells, AV +/PI+), Q2-3 (normal cells, AV-/PI−), and Q2-4 (early apoptotic cells, AV+/PI−). Heat map (F) describes the changes in the percent of cells in each quadrant among all the test groups. The highest percentage approaching 100% is indicated by the yellow squares and the lowest with numbers approaching 0–1% are observed as violet boxes. (*), (#) and ($) represent significant differences compared to the control, Cr and Cuo NPs treated groups, respectively. Statistical analysis was performed using one one-way ANOVA test with Tukey post hoc test. The existence of any of such symbols (*, #, and $) once refers to P-value ≤ 0.05, twice indicates P-value ≤ 0.01, and thrice means P-value ≤ 0.001.

Table 4 Cell cycle distribution of HCT-116 cells after receiving Cr, CuO NPs, and Cr@CuO NPs treatments for 48 h[a]

HCT-116 phase	Control (untreated)	Cr (8.24 μg mL^{-1})	CuO NPs (11.25 μg mL^{-1})	Cr@CuO NPs (5.17 μg mL^{-1})
Sub-G1	0.61 ± 0.29	1.01 ± 0.10	0.96 ± 0.10	$^{***\#\#\#\$\$\$}$2.88 ± 0.26
G1	34.70 ± 1.69	***19.24 ± 0.73	34.26 ± 1.17	$^{***\#\#\$\$\$}$24.26 ± 0.40
S	25.74 ± 0.85	***17.50 ± 0.79	**19.49 ± 1.52	$^{***\#\#\#\$\$\$}$8.42 ± 1.10
G2	25.02 ± 0.16	***59.27 ± 1.42	**37.27 ± 2.61	$^{***\$\$\$}$62.95 ± 1.44

[a] Data presented as mean ± SD. (*), (#) and ($) represent significant differences compared to the Control, Cr and Cuo NPs treated groups, respectively. Statistical analysis was performed using one one-way ANOVA test with Tukey post hoc test.

uncontrolled cell division occurs and cancer is induced.[78] In the current study, all treatment groups significantly arrested the cells at the G2 phase and stopped the G2/M transition relative to the control group. Cr@CuO NPs trapped even more cells at G2 phase than pure CuO NPs. Meanwhile, both Cr@CuO NPs and free Cr arrested a comparable or almost very similar cell population percentage at the G2 phase. Likewise, analysis of colon adenocarcinoma (CT-26) cells revealed a significant increase in the number of G2 phase cells following treatment with free Cr relative to the control (blank) cells.[79] Moreover, CuO NPs ability to arrest the cell cycle at G2 phase and prevent G2-M transition were previously reported in human lung cancer (A-549)[80] and skin cancer (A-375)[81] cells.

In a nutshell, the three treatments successfully decreased the percent cellular population undergoing DNA duplication in the S-phase and stopped the G2/M transition by trapping the cells at G2. Cr@CuO NPs possessed an additional effect by inducing cellular arrest at the Sub-G1 phase and towering up the effects

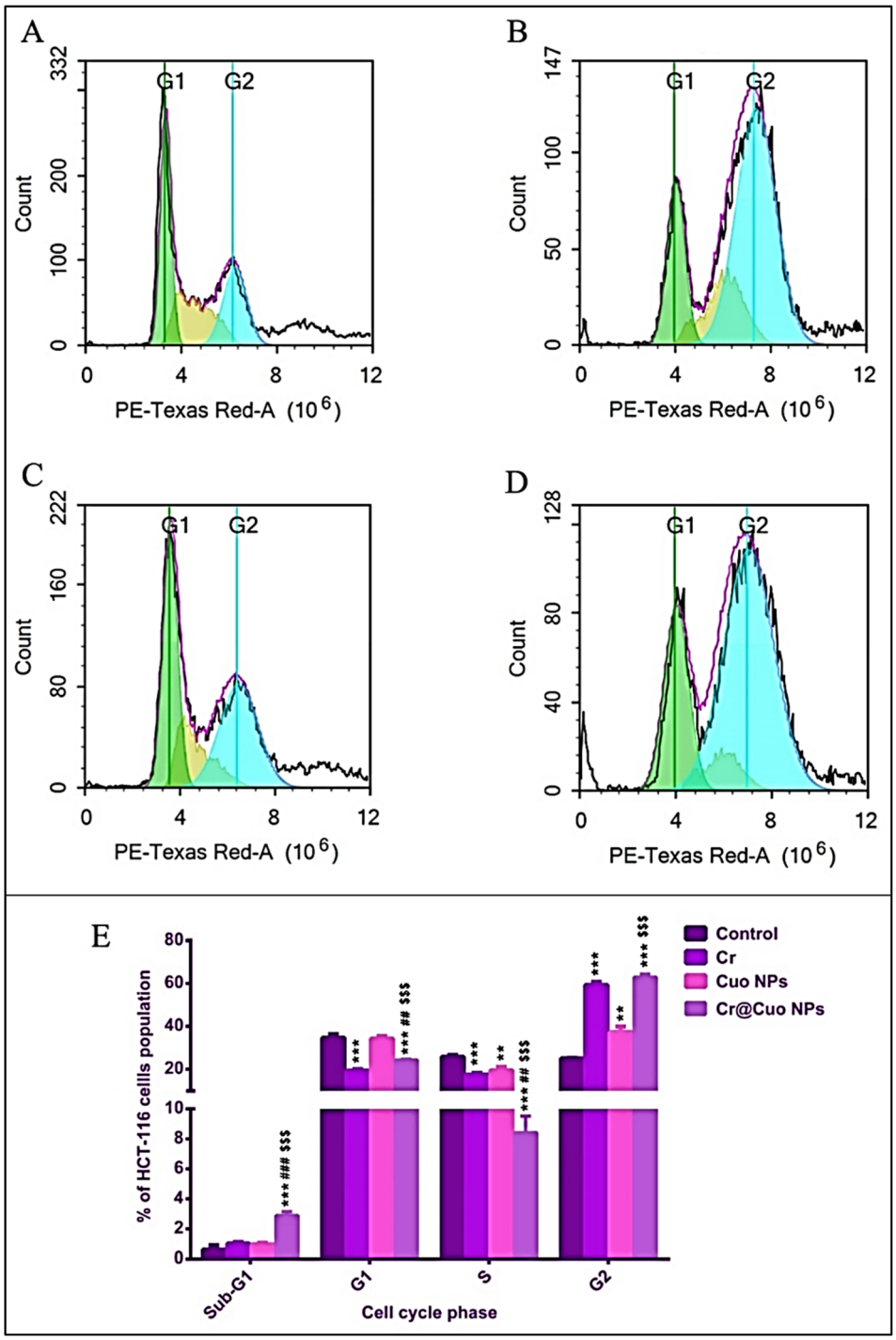

Fig. 9 Cell cycle analysis of untreated HCT-116 cells is shown in cytogram (A). The cytograms (B), (C), and (D) refer to the cell cycle of HCT-116 cells following 48 of exposure to Cr, CuO NPs, and Cr@CuO NPs, respectively. The bar graph (E) displays the percentage of HCT-116 cells and their distribution among the different phases of the cell cycle. *P*-values are presented as: ** ≤0.01 and *** ≤0.001 against control; ## ≤ 0.01 and ### ≤ 0.001 compared to Cr, $$$ ≤ 0.001 *vs.* CuO NPs.

of the other two treatments at both S and G2 phases whereby providing added evidence to the apoptosis assay results.

RT-qPCR. The Bcl-2 family of proteins, which include both pro-apoptotic members like Bax that increase mitochondrial permeability and anti-apoptotic members like Bcl-2 that block their effects or prevent the release of cyt c from mitochondria, play a major role in mediating the mitochondrial apoptotic process.[82,83] In the current study, the investigated treatments (Cr, CuO NPs, and Cr@CuO NPs) were provided to the cells at the estimated IC_{50} for 48 h. Then, RT-qPCR was performed to determine the relative gene expression of the pro-apoptotic (Bax) and anti-apoptotic (Bcl-2) genes, as well as the tumor

suppressor gene (p53) that regulates their activity. The assay aimed to provide further insights and a deeper description of our apoptotic findings at the molecular level.

In several cancers, including colon cancer, the repression of Bax gene has been linked to chemotherapy resistance and a bad prognosis.[84] The Cr treatment has previously demonstrated a significant ability to elevate the expression of Bax in several tumors, such as the human lymphoma Raji cell line[85] and breast cancer (MCF-7) cells.[86] CuO NPs were also noticed to induce Bax gene expression in human hepatocarcinoma HepG2,[87] and chronic myeloid leukemia K562,[88] cell lines. Herein, our study revealed a 2.4-fold and 1.6-fold elevation in the relative normalized gene expression of Bax in HCT-116 cells treated with Cr and CuO NPs, respectively. The synthesized Cr@CuO NPs caused a 3.5-fold increase in Bax expression. As reported in Fig. 10, the expression of Bax in Cr@CuO NPs treated cells significantly surpassed that of Cr ($P \leq 0.01$) and CuO NPs ($P \leq 0.001$) treated cells. This could be considered an additional proof of the apoptotic effects of Cr@CuO NPs at the molecular level, which is strongly supported by the noticeably increased levels of Bax.

Bcl-2 is a protein that inhibits apoptosis. The increase in the Bcl-2 gene product has been widely associated with resistance to chemotherapeutic agents in multiple colon cancer cell lines.[89] As opposed to the Bax gene, Cr treatment for 48 h resulted in a considerable reduction in the expression of Bcl-2 in the human lymphoma Raji cell line[85] and breast cancer (MCF-7) cells.[86]

Additionally, the Bcl-2 expression witnessed a remarkable downregulation in human hepatocarcinoma HepG2,[87] and chronic myeloid leukemia K562 cell lines[88] following CuO NPs treatment. Likewise, our findings showed that Cr and CuO NPs treatments significantly reduced the normalized gene expression of the anti-apoptotic marker, Bcl-2, by 39% and 45%, respectively (Fig. 10). The newly formulated Cr@CuO NPs treatment resulted in a more significant decline in Bcl-2 gene expression relative to Cr ($P \leq 0.001$) and CuO NPs ($P \leq 0.01$) (Fig. 10).

Since both the gain- and loss-of-its-function mutations have been observed in various tumors, the tumor suppressor gene, p53 has revealed a complex participation in the process of carcinogenesis.[90] The p53 gene is known to directly enhance the Bax gene transcription and hence, the production of Bax protein.[91] Cumulative studies have pointed to the ability of both Cr[86] and CuO NPs[87,88] treatments to produce a significant increase in the p53 gene expression, promoting that of the Bax gene in a variety of tumors. In the current study, treatment with both Cr and CuO NPs resulted in a noticeable increase in the relative normalized gene expression of p53 by 2.7 and 2.2 folds (Fig. 10). It is noteworthy that Cr@CuO NPs treatment resulted in a marked increase of p53 expression by 3.8 folds, which exceeded that of the other two treatments (Fig. 10).

The novel Cr@CuO NPs treatment displayed an unprecedented and surplus activity at increasing the p53-Bax mediated mitochondrial apoptosis and downregulating the expression of Bcl-2 compared to the single Cr or CuO NPs therapy. As such, Cr@CuO NPs are depicted to possess favorable therapeutic properties that are worth further preclinical and clinical trials in colon cancer.

Computational findings

Cr and CuO interaction analysis. The possible interaction between carboplatin and copper oxide was first studied using Discovery Studio 4.1 Software, where energy minimization was applied to both residues using CHARMm and Momany-Rone

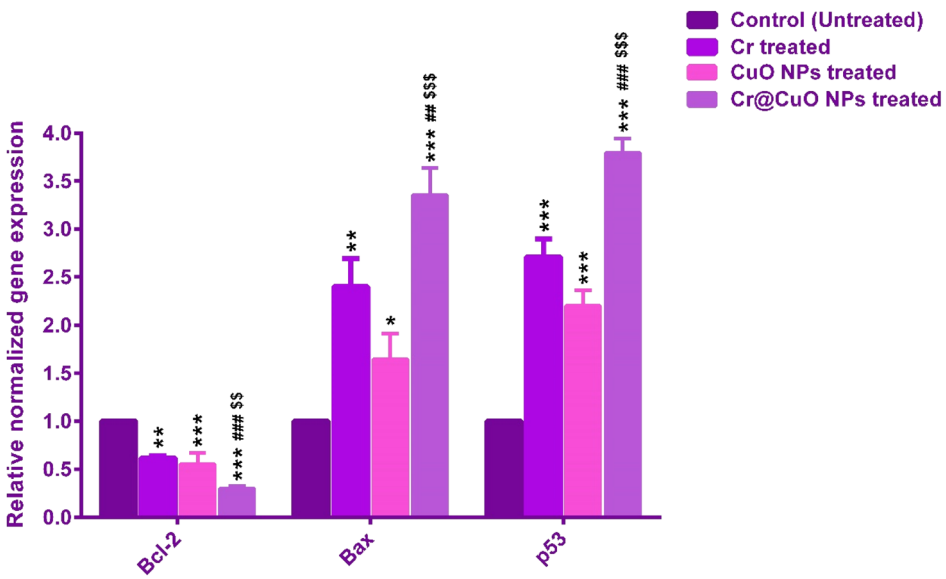

Fig. 10 RT-qPCR for the pro-apoptotic and anti-apoptotic genes in HCT-116 colon cancer cells after 48 h exposure to the test agents. The data is normalized to β-actin and presented as the average of triplicates ± standard deviation (SD). (*), (#) and ($) represent significant differences compared to the control, Cr and CuO NPs treated groups, respectively. The symbol presentation at once, twice, and thrice refer to ($P \leq 0.05$), ($P \leq 0.01$), and ($P \leq 0.001$), respectively.

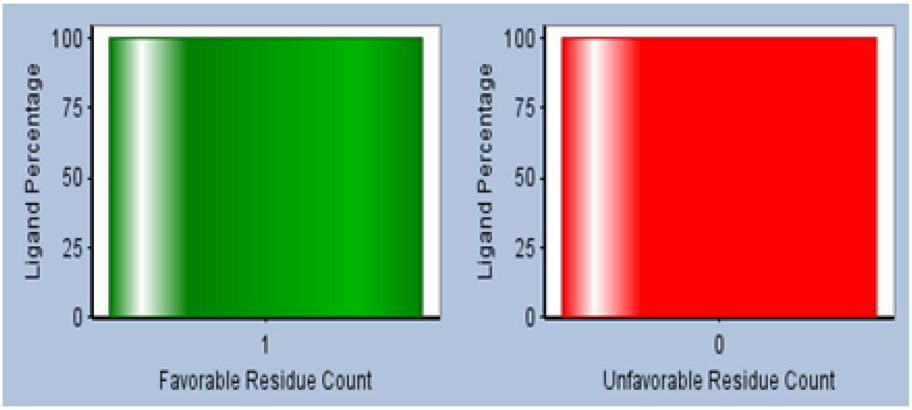

Fig. 11 Statistical residue analysis plot of the favorable (green) and unfavorable (orange) ratio of ligand (CuO) interaction with the receiver molecule (Cr).

forcefield and rendering Cr as a receiver molecule. The possible molecular ratio and possible charge were predicted *via* statistical residue analysis in ESI (Table S1).† The generated plots in Fig. 11 showed that the possible molecular ratio of interaction will be 1 : 1 and the unfavorable count of ligands will be zero. The interaction between Cr and CuO (Fig. 12) showed metal–ligand interaction between Pt and oxygen atom and two electrostatic interactions between Cu and each of the NH_3 groups of the Cr. The VDW interaction energy of the mixture obtained was -0.0019 kcal mol^{-1}, while the interaction energy of CuO is -18.6092 kcal mol^{-1} and that of cris -18.4248 kcal mol^{-1}. On the other hand, calculated *in situ* starting energy was $-67{,}404.2$ kcal mol^{-1}, *in situ* final energy after the interaction was -45.2372 kcal mol^{-1}, *in situ* gradient was 0.000696528 and free energy was -431.833 kcal mol^{-1}.

Molecular docking studies. To investigate more into the mechanism of anticancer activity of the mixture against colorectal type, human alanine aminotransferase 2 was selected. This potential target was chosen as a consequence of the approved literature theory, that elevated alanine aminotransferase (ALT) is frequently observed in subjects with metabolic syndrome, which is associated with the risk of colorectal adenoma (CRA).[92] The human alanine aminotransferase 2 crystal structure in complex with pyridoxal-5′-phosphate (PLP) was downloaded from RCSB Protein data bank with PDB ID 3IHJ.[93] The enzyme was cleaned and, missing residues were added and energy minimization was applied using the same forcefield applied to previous ligands. Utilizing Discovery Studio 4.1, C-docker protocol was adopted to generate molecular docking studies between enzyme and ligand as a reference compound and between enzyme and CuO, carboplatin and the mixture separately. Ten conformations of each ligand were generated and only the conformation with the least interaction energy was selected.

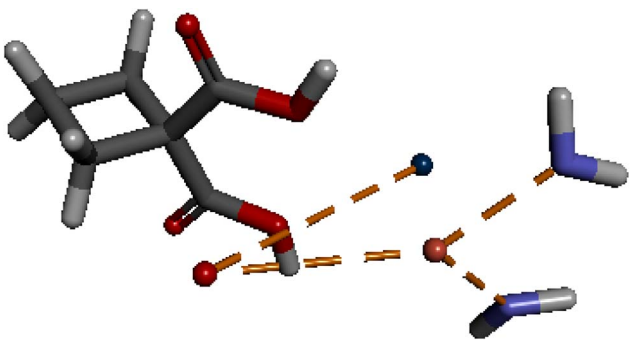

Fig. 12 3D interaction diagram between Cr and CuO. Orange dotted lines are indications of electrostatic interaction. Dark blue ball represents Pt metal and dark red ball represents Cu.

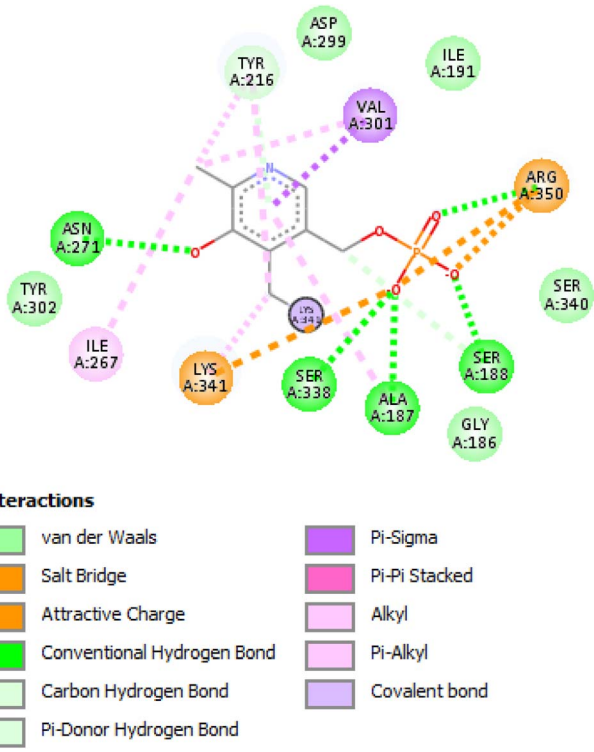

Fig. 13 2D interaction diagram between PLP and human alanine aminotransferase 2.

The results revealed that the reference compound PLP had −(C-docker interaction energy) = −22.5467 kcal mol^{-1}, and as shown in Fig. 13 PLP interacted with aminotransferase *via* attractive charge with Lys 341 and Pi-interactions with Val 301 and Tyr 216. Meanwhile, the interaction energies of CuO, Cr, and mixture were −32.2555, −43.2792, and −68.8381 kcal mol^{-1}, respectively. The 3D interaction diagrams between each ligand and enzyme in Fig. 14 illustrate the interaction of CuO *via* H-bond with Arg 494, and Val 478 and, another Pi-interaction with Arg 494, and a metal–ligand interaction between Cu and Asp177. This reflected a remote interaction than the binding site of CuO alone. At the same time, Cr showed two H-bonds with Lys 341, two H-bonds with Asp 386, H-bond with Pro 269, Glu 300, and Arg 134, together with Pi-interaction with Arg 134, Arg 137, Val 301, and Tyr 216 and finally Pt-ligand interaction with Pro 214, Asn 271 and Thr 273. That resulted in better interaction within the targeted binding site of the enzyme and better interaction energy. Furthermore, the mixture presented interactions as two H-bonds with Lys 341 and one H-bond with Gly 342, Pi-interaction with Val 301, Tyr 216, and Tyr 302, and metal–ligand interactions in the form of Cu and Gly 254 and Pt and Pro 269 and Gly 270. These results ensured that the binding mode of the mixture was the best among all ligands and had better stability from interaction energy. That correlated much with the *in vitro* cell line assay against colorectal cell lines that showed the most potent

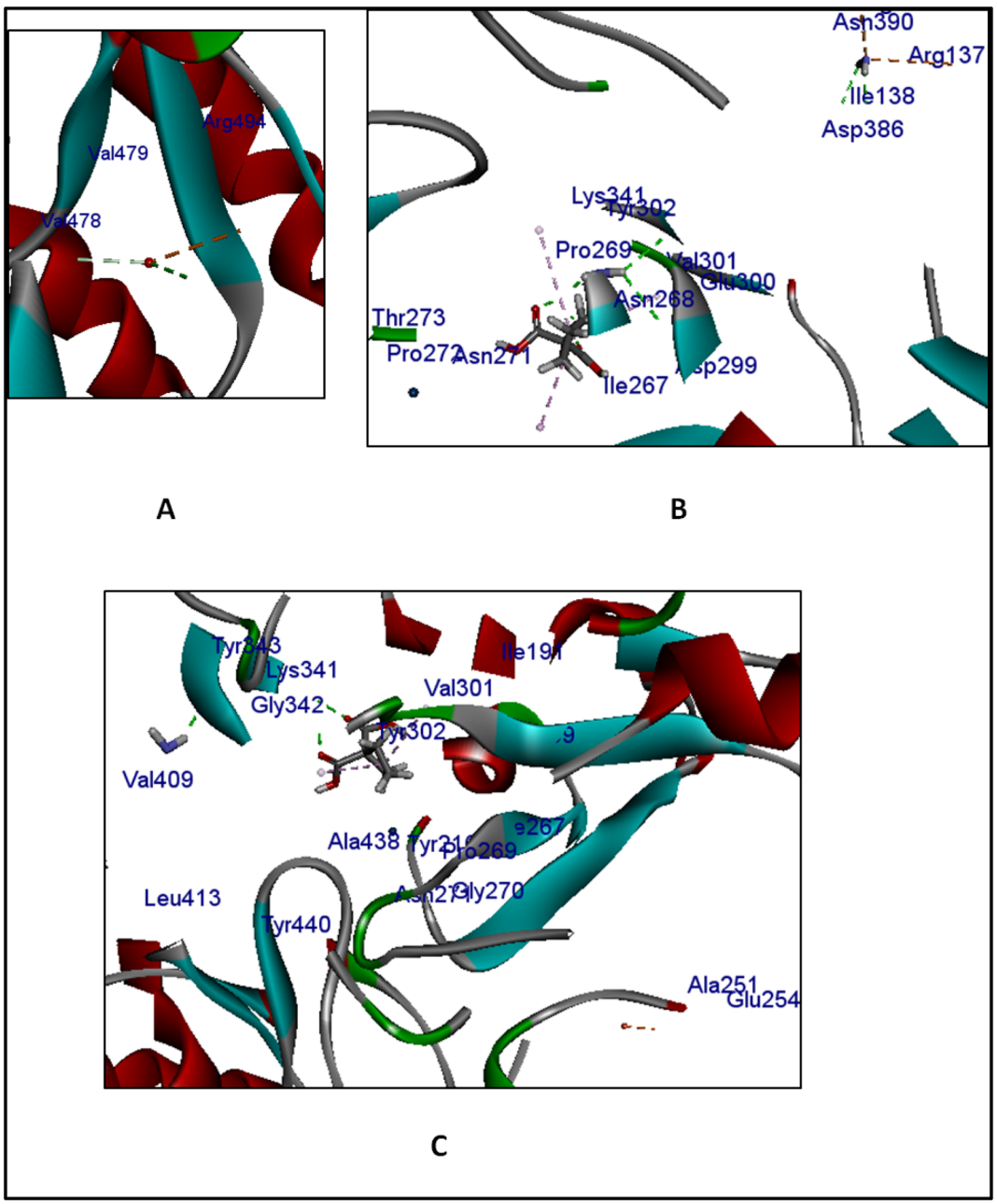

Fig. 14 3D interaction diagram between CuO (A), Cr (B), mixture (C) and aminotransferase enzyme.

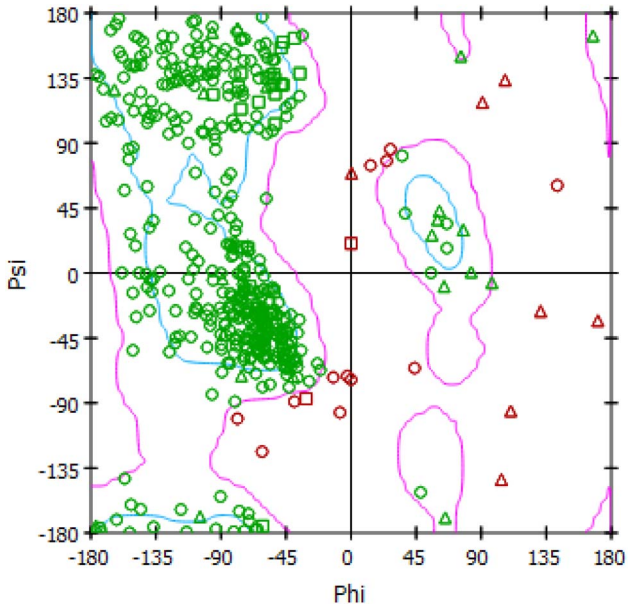

Fig. 15 Ramachandran plot representation of torsional energy conformations for interaction between mixture and human alanine aminotransferase 2. Green circles represent favorable areas, red triangles represent unfavorable areas, purple line represents an area outside binding sites, and blue line represents an area inside binding sites.

anticancer activity in the mixture form with CuO than individual CuO or Cr.

Ramachandran plot. In order to verify predicted torsion angles in the enzyme and confirm the interaction of the mixture in correct binding sites, a Ramachandran plot was generated, which indicates low energy conformations for φ (phi) and ψ (psi), the conventional terms used to represent the torsion angles on either side of alpha carbons in peptides. The graphical representation in Fig. 15 represented the local backbone conformation of each residue in the enzyme during interaction with the mixture. The plot showed multiple favorable areas in green where individual residues were likely to be built correctly.

Conclusions

In this work, we designed spherical NPs utilizing a facile and rapid microwave-assisted approach using *Boswellia carterii* essential oil extract. GC/MS analysis of the chemical composition of the extracted essential oil showed the abundancy of *trans*-nerolidol, verticiol, DL-limonene and linalool, which might be involved in the biosynthesis of CuO NPs by acting as reducing and capping agents. The loading of Cr onto the CuO NPs did not affect the spherical morphology of the CuO NPs, and had a high EE% and a triphasic release behavior into acidic pH, which simulated that of the tumor microenvironment. Several cellular and molecular biology assays were performed to assess the antitumor activity of Cr@CuO NPs, as well as its underlying mechanism of action. The results sounded very promising whereby Cr@CuO NPs imposed a superb cytotoxic activity against HCT-116 colon cancer cells as compared to free Cr or CuO NPs treatments. Moreover, Cr@CuO NPs succeeded at conserving the normal CCD841 CoN cells and attaining the highest selectivity index among all the investigated agents, rendering it of high therapeutic potential with minimal toxicity. The newly synthesized Cr@CuO NPs were superior to free Cr or CuO NPs by far in inducing apoptosis and cell cycle arrest at both sub-G1 and G2-phases of the cell cycle. Molecular biology investigations reflected the exquisite ability of Cr@CuO NPs to stimulate the gene expression of the pro-apoptotic markers p53 and Bax while downregulating Bcl-2. The insightful results suggest multiple benefits for using Cr@CuO NPs in the treatment of colon cancer.

Data availability

Data is contained within the article.

Conflicts of interest

The authors declare no conflict of interest.

Acknowledgements

This work was funded by the RSC Research Fund grant (ID: R22-3870733873) from the Royal Society of Chemistry to Dr Sherif Ashraf Fahmy. The authors are thankful to the Deanship of Scientific Research at King Khalid University in Abha, Saudi Arabia, for partial funding of parts of this work through large groups (project under grant number R.G.P. 1/430/44).

References

1 M. Ahmed, Colon Cancer: A Clinician's Perspective in 2019, *Gastroenterol. Res.*, 2020, **13**, 1–10, DOI: **10.14740/gr1239**.
2 X. Li, D. Wen, X. Li, C. Yao, W. Chong and H. Chen, Identification of an Immune Signature Predicting Prognosis Risk and Lymphocyte Infiltration in Colon Cancer, *Front. Immunol.*, 2020, **11**, 1–13, DOI: **10.3389/fimmu.2020.01678**.
3 A. Esmeeta, S. Adhikary, V. Dharshnaa, P. Swarnamughi, Z. Ummul Maqsummiya, A. Banerjee, S. Pathak and A. K. Duttaroy, Plant-derived bioactive compounds in colon cancer treatment: an updated review, *Biomed. Pharmacother.*, 2022, **153**, 113384, DOI: **10.1016/j.biopha.2022.113384**.
4 T. Hu, Z. Li, C. Y. Gao and C. H. Cho, Mechanisms of drug resistance in colon cancer and its therapeutic strategies, *World J. Gastroenterol.*, 2016, **22**, 6876–6889, DOI: **10.3748/wjg.v22.i30.6876**.
5 G. F. de Sousa, S. R. Wlodarczyk and G. Monteiro, Carboplatin: molecular mechanisms of action associated with chemoresistance, *Braz. J. Pharm. Sci.*, 2014, **50**, 693–702, DOI: **10.1590/S1984-82502014000400004**.
6 N. Aissat, C. Le Tourneau, A. Ghoul, M. Serova, I. Bieche, F. Lokiec, E. Raymond and S. Faivre, Antiproliferative effects of rapamycin as a single agent and in combination with carboplatin and paclitaxel in head and neck cancer

cell lines, *Cancer Chemother. Pharmacol.*, 2008, **62**, 305–313, DOI: 10.1007/s00280-007-0609-2.

7 T. Chen, M. Li, R. Zhang and H. Wang, Dihydroartemisinin induces apoptosis and sensitizes human ovarian cancer cells to carboplatin therapy, *J. Cell. Mol. Med.*, 2009, **13**, 1358–1370, DOI: 10.1111/j.1582-4934.2008.00360.x.

8 P. A. Bunn Jr, Review of therapeutic trials of carboplatin in lung cancer, *Semin. Oncol.*, 1989, **16**, 27–33.

9 H. I. Bahr, A. T. Ibrahiem, A. M. Gabr, A. M. Elbahaie, H. S. Elmahdi, N. Soliman, A. M. Youssef, M. El-Sherbiny and S. A. Zaitone, Chemopreventive effect of α-hederin/carboplatin combination against experimental colon hyperplasia and impact on JNK signaling, *Toxicol. Mech. Methods*, 2021, **31**, 138–149, DOI: 10.1080/15376516.2020.1849483.

10 S. Danışman-Kalındemirtaş, F. Kariper, İ. A. Erdemir, G. Sert and E. Erdem-Kuruca, Evaluation of anticancer effects of carboplatin–gelatin nanoparticles in different sizes synthesized with newly self-assembly method by exposure to IR light, *Sci. Rep.*, 2022, **12**(1), 10686.

11 F. A. Khan, R. Albalawi and F. H. Pottoo, Trends in targeted delivery of nanomaterials in colon cancer diagnosis and treatment, *Med. Res. Rev.*, 2022, **42**, 227–258, DOI: 10.1002/med.21809.

12 N. A. Bhaskaran and L. Kumar, Treating colon cancers with a non-conventional yet strategic approach: an overview of various nanoparticulate systems, *J. Controlled Release*, 2021, **336**, 16–39, DOI: 10.1016/j.jconrel.2021.06.008.

13 S. Tabrez, A. U. Khan, A. A. Mirza, M. Suhail, N. R. Jabir, T. A. Zughaibi and M. Alam, Biosynthesis of copper oxide nanoparticles and its therapeutic efficacy against colon cancer, *Nanotechnol. Rev.*, 2022, **11**, 1322–1331, DOI: 10.1515/ntrev-2022-0081.

14 A. N. Harbi and K. H. Abd, Biosynthesis of CuO NPs and its anticancer activity on human colon cancer cell lines (HT-29), *J. Phys.: Conf. Ser.*, 2021, **1963**, 012151, DOI: 10.1088/1742-6596/1963/1/012151.

15 G. Go, C. S. Lee, Y. M. Yoon, J. H. Lim, T. H. Kim and S. H. Lee, Prpc aptamer conjugated–gold nanoparticles for targeted delivery of doxorubicin to colorectal cancer cells, *Int. J. Mol. Sci.*, 2021, **22**, 1–16, DOI: 10.3390/ijms22041976.

16 Y. Wang, P. Li, L. Chen, W. Gao, F. Zeng and L. X. Kong, Targeted delivery of 5-fluorouracil to HT-29 cells using high efficient folic acid-conjugated nanoparticles, *Drug Delivery*, 2015, **22**, 191–198, DOI: 10.3109/10717544.2013.875603.

17 P. Gogoi, G. Kaur and N. K. Singh, Nanotechnology for colorectal cancer detection and treatment, *World J. Gastroenterol.*, 2022, **28**, 6497–6511, DOI: 10.3748/wjg.v28.i46.6497.

18 B. Brar, K. Ranjan, A. Palria, R. Kumar, M. Ghosh, S. Sihag and P. Minakshi, Nanotechnology in Colorectal Cancer for Precision Diagnosis and Therapy, *Front. Nanotechnol.*, 2021, **3**, 1–21, DOI: 10.3389/fnano.2021.699266.

19 D. Solairaj, P. Rameshthangam and G. Arunachalam, Anticancer activity of silver and copper embedded chitin nanocomposites against human breast cancer (MCF-7) cells, *Int. J. Biol. Macromol.*, 2017, **105**, 608–619, DOI: 10.1016/j.ijbiomac.2017.07.078.

20 J. He, R. Song, F. Xiao, M. Wang and L. Wen, Cu3 P/1-MT Nanocomposites Potentiated Photothermal-Immunotherapy, *Int. J. Nanomed.*, 2023, **18**, 3021–3033, DOI: 10.2147/IJN.S414117.

21 R. S. Lanje, A. S. Sharma, S. J. Pode and R. B. Ningthoujam, Synthesis and optical characterization of copper oxide nanoparticles, *Adv. Appl. Sci. Res.*, 2010, **1**, 36–40.

22 S. Naz, A. Gul, M. Zia and R. Javed, Synthesis, biomedical applications, and toxicity of CuO nanoparticles, *Appl. Microbiol. Biotechnol.*, 2023, **107**, 1039–1061, DOI: 10.1007/s00253-023-12364-z.

23 E. Nagaraj, K. Karuppannan, P. Shanmugam and S. Venugopal, Exploration of Bio-synthesized Copper Oxide Nanoparticles Using Pterolobium hexapetalum Leaf Extract by Photocatalytic Activity and Biological Evaluations, *J. Cluster Sci.*, 2019, **30**, 1157–1168, DOI: 10.1007/s10876-019-01579-8.

24 N. Al-Jawhari, H. Bin-Thiyab and H. Elbialy, In vitro antioxidant and anticancer activities of cupric oxide nanoparticles synthesized using spinach leaves extract, *Nano-Struct. Nano-Objects*, 2022, **29**, 100815.

25 V. Gnanavel, V. Palanichamy and S. M. Roopan, Biosynthesis and characterization of copper oxide nanoparticles and its anticancer activity on human colon cancer cell lines (HCT-116), *J. Photochem. Photobiol., B*, 2017, **171**, 133–138, DOI: 10.1016/j.jphotobiol.2017.05.001.

26 K. Huang, Y. Chen, K. Liang, X. Xu, J. Jiang, M. Liu and F. Zhou, Review of the Chemical Composition, Pharmacological Effects, Pharmacokinetics, and Quality Control of Boswellia carterii, *Evid.-Based Complementary Altern. Med.*, 2022, **2022**, 6627104, DOI: 10.1155/2022/6627104.

27 J. J. Liu and R. D. Duan, LY294002 enhances boswellic acid-induced apoptosis in colon cancer cells, *Anticancer Res.*, 2009, **29**, 2987–2991.

28 M. M. Suhail, W. Wu, A. Cao, F. G. Mondalek, K. M. Fung, P. T. Shih, Y. T. Fang, C. Woolley, G. Young and H. K. Lin, Boswellia sacra essential oil induces tumor cell-specific apoptosis and suppresses tumor aggressiveness in cultured human breast cancer cells, *BMC Complementary Altern. Med.*, 2011, **11**, 129, DOI: 10.1186/1472-6882-11-129.

29 E. Becer, H. Kabadayı, K. H. C. Başer and H. S. Vatansever, Boswellia sacra essential oil manages colon cancer stem cells proliferation and apoptosis: a new perspective for cure, *J. Essent. Oil Res.*, 2021, **33**, 53–62, DOI: 10.1080/10412905.2020.1839586.

30 N. O. Makarov, V. V. Love, A. J. Sinitsyna, O. V. Makarova, S. S. Yaminsky, I. V. Taliansky and M. E. Kalinina, "Green" nanotechnologies: synthesis of metal nanoparticles using plants, *Acta Nature*, 2014, **6**, 35–44, DOI: 10.4135/9781452231631.n3.

31 H. M. E. S. Azzazy, A. Abdelnaser, H. Al Mulla, A. M. Sawy, S. N. Shamma, M. Elhusseiny, S. Alwahibi, N. K. Mahdy and S. A. Fahmy, Essential Oils Extracted from Boswellia sacra Oleo Gum Resin Loaded into PLGA-PCL

Nanoparticles: Enhanced Cytotoxic and Apoptotic Effects against Breast Cancer Cells, *ACS Omega*, 2022, 2–10, DOI: 10.1021/acsomega.2c06390.

32 M. Elyemni, B. Louaste, I. Nechad, T. Elkamli, A. Bouia, M. Taleb, M. Chaouch and N. Eloutassi, Extraction of Essential Oils of Rosmarinus officinalis L. by Two Different Methods: Hydrodistillation and Microwave Assisted Hydrodistillation, *Sci. World J.*, 2019, **2019**, 3659432, DOI: 10.1155/2019/3659432.

33 S. E. Stein, P. Ausloos and S. G. Lias, Comparative Evaluations of Mass Spectral Databases, *J. Am. Soc. Mass Spectrom.*, 1991, **2**, 441–443, DOI: 10.1016/1044-0305(91)85012-U.

34 R. Oprean, L. Oprean, M. Tamas, R. Sandulescu and L. Roman, Essential oils analysis. II. Mass spectra identification of terpene and phenylpropane derivatives, *J. Pharm. Biomed. Anal.*, 2001, **24**, 1163–1168, DOI: 10.1016/S0731-7085(00)00578-1.

35 C. Mallikarjunaswamy, V. Lakshmi Ranganatha, R. Ramu, Udayabhanu and G. Nagaraju, Facile microwave-assisted green synthesis of ZnO nanoparticles: application to photodegradation, antibacterial and antioxidant, *J. Mater. Sci.: Mater. Electron.*, 2020, **31**, 1004–1021, DOI: 10.1007/s10854-019-02612-2.

36 S. A. Fahmy, I. M. Fawzy, B. M. Saleh, M. Y. Issa, U. Bakowsky and H. M. E. S. Azzazy, Green synthesis of platinum and palladium nanoparticles using Peganum harmala L. Seed alkaloids: biological and computational studies, *Nanomaterials*, 2021, **11**, 1–15, DOI: 10.3390/nano11040965.

37 S. A. Fahmy, A. Ramzy, A. M. Sawy, M. Nabil, M. Z. Gad, M. El-Shazly, M. A. M. Aboul-soud and H. M. E. Azzazy, Ozonated Olive Oil: Enhanced Cutaneous Delivery via Niosomal Nanovesicles for Melanoma Treatment, *Antioxidants*, 2022, **11**, 1318, DOI: 10.3390/antiox11071318.

38 N. K. Mahdy, M. El-Sayed, S. E. D. Al-Mofty, A. Mohamed, A. H. Karaly, M. E. El-Naggar, H. Nageh, W. A. Sarhan and H. M. E. S. Azzazy, Toward Scaling up the Production of Metal Oxide Nanoparticles for Application on Washable Antimicrobial Cotton Fabrics, *ACS Omega*, 2022, **7**, 38942–38956, DOI: 10.1021/acsomega.2c04692.

39 S. Talam, S. R. Karumuri and N. Gunnam, Synthesis, Characterization, and Spectroscopic Properties of ZnO Nanoparticles, *ISRN Nanotechnol.*, 2012, 1–6, DOI: 10.5402/2012/372505.

40 S. A. Fahmy, M. Y. Issa, B. M. Saleh, M. R. Meselhy and H. M. E. S. Azzazy, Peganum harmala alkaloids self-assembled supramolecular nanocapsules with enhanced antioxidant and cytotoxic activities, *ACS Omega*, 2021, **6**, 11954–11963, DOI: 10.1021/acsomega.1c00455.

41 S. M. Abdel-Hafez, R. M. Hathout and O. A. Sammour, Tracking the transdermal penetration pathways of optimized curcumin-loaded chitosan nanoparticles via confocal laser scanning microscopy, *Int. J. Biol. Macromol.*, 2018, **108**, 753–764, DOI: 10.1016/j.ijbiomac.2017.10.170.

42 M. X. Chen, T. Li, S. Peng and D. Tao, Supramolecular nanocapsules from the self-assembly of amphiphilic calixarene as a carrier for paclitaxel, *New J. Chem.*, 2016, **40**, 9923–9929, DOI: 10.1039/c6nj01986b.

43 N. K. Sedky, N. M. Abdel-kader, M. Y. Issa, M. M. M. Abdelhady, S. N. Shamma, U. Bakowsky and S. A. Fahmy, Co-Delivery of Ylang Ylang Oil of Cananga odorata and Oxaliplatin Using Intelligent pH-Sensitive Lipid-Based Nanovesicles for the Effective Treatment of Triple-Negative Breast Cancer, *Int. J. Mol. Sci.*, 2023, **24**(9), 8392, DOI: 10.3390/ijms24098392.

44 S. A. Fahmy, N. K. Sedky, A. Ramzy, M. M. M. Abdelhady, O. Abd, A. Alabrahim, S. N. Shamma, H. Mohamed and E. Azzazy, Green extraction of essential oils from Pistacia lentiscus resins: Encapsulation into Niosomes showed improved preferential cytotoxic and apoptotic effects against breast and ovarian cancer cells, *J. Drug Delivery Sci. Technol.*, 2023, **87**, 104820, DOI: 10.1016/j.jddst.2023.104820.

45 K. Sarkar, J. Chakraborty, N. Chatterjee, A. Bhattacharjee, A. Dasgupta and D. Acharya, Green Synthesized Copper Oxide Nanoparticles Ameliorate Defence and Antioxidant Enzymes in Lens culinaris, *Nanomaterials*, 2020, 1–27.

46 N. Anandhavalli, B. Mol, S. Manikandan, N. Anusha, V. Ponnusami and K. S. Rajan, Green synthesis of cupric oxide nanoparticles using water extract of Murrya koenigi and its photocatalytic activity, *Asian J. Chem.*, 2015, **27**, 2523–2526, DOI: 10.14233/ajchem.2015.17966.

47 N. M. Aboeita, S. A. Fahmy, M. M. H. El-Sayed, H. M. E. S. Azzazy and T. Shoeib, Enhanced Anticancer Activity of Nedaplatin Loaded onto Copper Nanoparticles Synthesized Using Red Algae, *Pharmaceutics*, 2022, **14**(2), 418, DOI: 10.3390/pharmaceutics14020418.

48 A. A. A. Go and S. Ronald, Review of the Comparative Pharmacology and Clinical Activity of Cisplatin and Carboplatin, *J. Clin. Oncol.*, 2016, **17**, 409–422.

49 A. O. Fatimah, R. I. Alharbi, G. Albasher, R. Almeer and N. S. Alsaggabi, Antifungal Potential of Aqueous Extract of Boswellia carteri, *J. Pure Appl. Microbiol.*, 2019, **13**, 2375–2381, DOI: 10.22207/JPAM.13.4.53.

50 F. M. Fakhree, I. F. Waheed and K. M. Mahmoud, Synthesis and characterization of Cuo nanoparticles stabilized by quercetin and its application for anti-breast cancer activity, *Egypt. J. Chem.*, 2021, **64**, 2989–2995, DOI: 10.21608/ejchem.2021.56260.3207.

51 R. I. Iliescu, E. Andronescu, C. D. Ghiţulică, D. Berger and A. Ficai, Montmorillonite-alginate nanocomposite beads as drug carrier for oral administration of carboplatin-preparation and characterization, *U.P.B. Sci. Bull., Series B*, 2011, **73**, 3–16.

52 M. A. Khan, M. Zafaryab, S. H. Mehdi, J. Quadri and M. M. A. Rizvi, Characterization and carboplatin loaded chitosan nanoparticles for the chemotherapy against breast cancer in vitro studies, *Int. J. Biol. Macromol.*, 2017, **97**, 115–122, DOI: 10.1016/j.ijbiomac.2016.12.090.

53 V. V. T. Padil and M. Černík, Green synthesis of copper oxide nanoparticles using gum karaya as a biotemplate and their antibacterial application, *Int. J. Nanomed.*, 2013, **8**, 889–898, DOI: 10.2147/IJN.S40599.

54 D. Das, B. C. Nath, P. Phukon and S. K. Dolui, Synthesis and evaluation of antioxidant and antibacterial behavior of CuO nanoparticles, *Colloids Surf., B*, 2013, **101**, 430–433, DOI: 10.1016/j.colsurfb.2012.07.002.

55 S. Sindhwani, A. M. Syed, J. Ngai, B. R. Kingston, L. Maiorino, J. Rothschild, P. MacMillan, Y. Zhang, N. U. Rajesh, T. Hoang, J. L. Y. Wu, S. Wilhelm, A. Zilman, S. Gadde, A. Sulaiman, B. Ouyang, Z. Lin, L. Wang, M. Egeblad and W. C. W. Chan, The entry of nanoparticles into solid tumours, *Nat. Mater.*, 2020, **19**, 566–575, DOI: 10.1038/s41563-019-0566-2.

56 S. M. Narum, T. Le, D. P. Le, J. C. Lee, N. D. Donahue, W. Yang and S. Wilhelm, Passive targeting in nanomedicine: fundamental concepts, body interactions, and clinical potential, in *Nanoparticles for Biomedical Applications: Fundamental Concepts, Biological Interactions and Clinical Applications*, Elsevier, 2019, pp. 37–53, DOI: 10.1016/B978-0-12-816662-8.00004-7.

57 A. A. Umar and M. Oyama, A seed-mediated growth method for vertical array of single-crystalline CuO nanowires on surfaces, *Cryst. Growth Des.*, 2007, **7**, 2404–2409, DOI: 10.1021/cg0602008.

58 M. Naz, N. Nasiri, M. Ikram, M. Nafees, M. Z. Qureshi, S. Ali and A. Tricoli, Eco-friendly biosynthesis, anticancer drug loading and cytotoxic effect of capped ag-nanoparticles against breast cancer, *Appl. Nanosci.*, 2017, **7**, 793–802, DOI: 10.1007/s13204-017-0615-6.

59 M. Bruschi, Main mechanisms to control the drug release, in *Strategies to Modify the Drug Release from Pharmaceutical Systems*, 2015, pp. 37–62, DOI: 10.1016/B978-0-08-100092-2.00004-7.

60 A. T. Alex, A. Joseph, G. Shavi, J. V. Rao, A. T. Alex, A. Joseph, G. Shavi, J. V. Rao and N. Udupa, Development and evaluation of carboplatin- loaded PCL nanoparticles for intranasal delivery development and evaluation of carboplatin-loaded PCL nanoparticles for intranasal delivery, *Drug Delivery*, 2016, **23**(7), 2144–2153, DOI: 10.3109/10717544.2014.948643.

61 S. Ranghar, P. Sirohi, P. Verma and V. Agarwal, Nanoparticle-based Drug Delivery Systems: Promising Approaches Against Infections, *Braz. Arch. Biol. Technol.*, 2014, **57**, 209–222.

62 Y. H. Hsueh, P. H. Tsai and K. S. Lin, pH-dependent antimicrobial properties of copper oxide nanoparticles in Staphylococcus aureus, *Int. J. Mol. Sci.*, 2017, **18**(4), 793, DOI: 10.3390/ijms18040793.

63 M. H. Karimi, G. R. Mahdavinia and B. Massoumi, pH-controlled sunitinib anticancer release from magnetic chitosan nanoparticles crosslinked with κ-carrageenan, *Mater. Sci. Eng., C*, 2018, **91**, 705–714, DOI: 10.1016/j.msec.2018.06.019.

64 U. Luesakul, S. Puthong, N. Neamati and N. Muangsin, pH-responsive selenium nanoparticles stabilized by folate-chitosan delivering doxorubicin for overcoming drug-resistant cancer cells, *Carbohydr. Polym.*, 2018, **181**, 841–850, DOI: 10.1016/j.carbpol.2017.11.068.

65 R. B. Badisa, S. F. Darling-reed, P. Joseph, J. S. Cooperwood, L. M. Latinwo and C. B. Goodman, Selective Cytotoxic Activities of Two Novel Synthetic Drugs on Human Breast Carcinoma MCF-7 Cells, *Anticancer Res.*, 2009, **2996**, 2993–2996.

66 P. Francielli, D. Oliveira, J. Morais, J. Lopes, R. Aparecida, M. Oliveira, H. Júnior, A. Eduardo, M. Crotti and D. Crispim, Cytotoxicity screening of essential oils in cancer cell lines, *Rev. Bras. Farmacogn.*, 2015, **25**, 183–188, DOI: 10.1016/j.bjp.2015.02.009.

67 Z. S. El Fakharany, Y. M. Nissan, N. K. Sedky, R. K. Arafa and S. M. A. Seri, New proapoptotic chemotherapeutic agents based on the quinolone - 3 - carboxamide scaffold acting by VEGFR - 2 inhibition, *Sci. Rep.*, 2023, 1–22, DOI: 10.1038/s41598-023-38264-w.

68 T. Sadhukha and S. Prabha, Encapsulation in Nanoparticles Improves Anti-cancer Efficacy of Carboplatin, *AAPS PharmSciTech*, 2014, **15**(4), 1029–1038, DOI: 10.1208/s12249-014-0139-2.

69 H. Eg and P. Aa, Copper Nanoparticles as Therapeutic Anticancer Agents Copper Nanoparticles as Therapeutic Anticancer Agents, *J. Nanomed. Nanotechnol.*, 2018, **2**(1), 119.

70 A. I. Journal, S. Pairoj, P. Damrongsak, B. Damrongsak, R. Kaewkhaw, C. Ruttanasirawit and K. Locharoenrat, Antitumor activities of carboplatin – doxorubicin – ZnO complexes in different human cancer cell lines (breast, cervix uteri, colon, liver and oral) under UV exposition, *Artif. Cells, Nanomed., Biotechnol.*, 2021, **49**, 120–135, DOI: 10.1080/21691401.2021.1876718.

71 S. M. Aborehab, N. M. Abd-Elmawla, M. A. ElSayed, A. M. Sabry and O. Ezzat, Acovenoside A as a novel therapeutic approach to boost taxol and carboplatin apoptotic and antiproliferative activities in NSCLC: interplay of miR-630/miR-181a and apoptosis genes, *Bioorg. Chem.*, 2023, **139**, 106743.

72 S. Vidot, J. Witham, R. Agarwal, S. Greenhough, H. S. Bamrah, G. J. Tigyi, S. B. Kaye and A. Richardson, Autotaxin delays apoptosis induced by carboplatin in ovarian cancer cells, *Cell Signal.*, 2010, **22**, 926–935, DOI: 10.1016/j.cellsig.2010.01.017.

73 S. Singh, A. K. Upadhyay, A. K. Ajay, M. K. Bhat, F. Zschunke, N. Miosge, P. Thelen and T. Schlott, p53 regulates ERK activation in carboplatin induced apoptosis in cervical carcinoma : a novel target of p53 in apoptosis, *FEBS Lett.*, 2007, **581**, 289–295, DOI: 10.1016/j.febslet.2006.12.035.

74 K. Ali, Q. Saquib, B. Ahmed, M. A. Siddiqui, J. Ahmad, M. Al-shaeri, A. A. Al-khedhairy and J. Musarrat, Bio-functionalized CuO nanoparticles induced apoptotic activities in human breast carcinoma cells and toxicity against Aspergillus fl avus : An in vitro approach, *Process Biochem.*, 2020, **91**, 387–397, DOI: 10.1016/j.procbio.2020.01.008.

75 P. C. Nagajyothi, P. Muthuraman, T. V. M. Sreekanth, D. Hwan and J. Shim, Green synthesis: in vitro anticancer activity of copper oxide nanoparticles against human cervical carcinoma cells, *Arabian J. Chem.*, 2017, **10**, 215–225, DOI: 10.1016/j.arabjc.2016.01.011.

76 P. Pozarowski and Z. Darzynkiewicz, Analysis of Cell Cycle by Flow Cytometry, *Checkpoint Controls and Cancer 2*, Activat, 2004, pp. 301–311.
77 M. Park and S. Lee, Cell Cycle and Cancer, *J. Biochem. Mol. Biol.*, 2003, **36**, 60–65.
78 G. H. Williams and K. Stoeber, The cell cycle and cancer, *J. Pathol.*, 2012, 352–364, DOI: **10.1002/path.3022**.
79 X. Zhu, Y. Peng and L. Qiu, Amino-functionalized nano-vesicles for enhanced anticancer efficacy and reduced myelotoxicity of carboplatin, *Colloids Surf., B*, 2017, **157**, 56–64, DOI: **10.1016/j.colsurfb.2017.05.041**.
80 M. Hanagata, N. Zhuang, F. Connolly, S. Li, J. Ogawa and N. Xu, Molecular Responses of Human Lung Epithelial Cells to the Toxicity of Copper Oxide Nanoparticles Inferred from Whole Genom Expression Analysis, *J. Am. Chem. Soc.*, 2011, 9326–9338.
81 S. Shahriary, F. Tafvizi, P. Khodarahmi and M. Shaabanzadeh, Phyto - Mediated Synthesis of CuO Nanoparticles Using Aqueous Leaf Extract of Artemisia Deserti and Their Anticancer Effects on A2780 - CP Cisplatin - Resistant Ovarian Cancer Cells, *Biomass Convers. Biorefin.*, 2022, **14**, 2263–2279, DOI: **10.1007/s13399-022-02436-x**.
82 E. Z. Bagci, Y. Vodovotz, T. R. Billiar, G. B. Ermentrout and I. Bahar, Bistability in Apoptosis : Roles of Bax , Bcl-2 , and Mitochondrial Permeability Transition Pores, *Biophys. J.*, 2006, **90**, 1546–1559, DOI: **10.1529/biophysj.105.068122**.
83 N. K. Sedky, M. Braoudaki, K. Mahdy, K. Amin, I. M. Fawzy, E. K. Efthimiadou, A. Youness and S. A. Fahmy, Box–Behnken design of thermo-responsive nano- liposomes loaded with a platinum(IV) anticancer complex: evaluation of cytotoxicity and apoptotic pathways in triple negative breast cancer cells, *Nanoscale Adv.*, 2023, **5**, 5399–5413, DOI: **10.1039/d3na00368j**.
84 M. Manoochehri and A. Karbasi, Down-Regulation of BAX Gene During Carcinogenesis and Acquisition of Resistance to 5-FU in Colorectal Cancer, *Pathol. Oncol. Res.*, 2014, 301–307, DOI: **10.1007/s12253-013-9695-0**.
85 P. Lin, B. Zhou, H. Yao and Y. Guo, Effect of carboplatin injection on Bcl-2 protein expression and apoptosis induction in Raji cells on om m er ci al us e on m al, *Eur. J. Histochem.*, 2020, **64**, 3134.
86 N. M. Aborehab, M. R. Elnagar and N. E. Waly, Gallic acid potentiates the apoptotic effect of paclitaxel and carboplatin via overexpression of Bax and P53 on the MCF - 7 human breast cancer cell line, *J. Biochem. Mol. Toxicol.*, 2021, 1–11, DOI: **10.1002/jbt.22638**.
87 M. A. Siddiqui, H. A. Alhadlaq, J. Ahmad, A. A. Al-khedhairy, J. Musarrat and M. Ahamed, Copper Oxide Nanoparticles Induced Mitochondria Mediated Apoptosis in Human Hepatocarcinoma Cells, *PLoS One*, 2013, **8**(8), e69534, DOI: **10.1371/journal.pone.0069534**.
88 M. Shafagh, F. Rahmani and N. Delirezh, CuO nanoparticles induce cytotoxicity and apoptosis in human K562 cancer cell line via mitochondrial pathway, through reactive oxygen species and P53, *Iran. J. Basic Med. Sci.*, 2015, **18**, 993–1000.
89 T. Violette, S. Poulain, L. Dussaulx, E. Pepin, D. Faussat, A. M. Chambaz, J. Lacorte, J. M. Staedel and C. Lesuffleur, Resistance of colon cancer cells to long-term 5-fluorouracil exposure is correlated to the relative level of Bcl-2 and Bcl-XL in addition to Bax and p53 status, *Int. J. Cancer*, 2002, **504**, 498–504, DOI: **10.1002/ijc.10146**.
90 A. J. Levine, W. Hu and Z. Feng, The P53 pathway : what questions remain to be explored, *Cell Death Differ.*, 2006, 1027–1036, DOI: **10.1038/sj.cdd.4401910**.
91 M. T. Hemann and S. W. Lowe, The P53 – Bcl-2 Connection, *Cell Death Differ*, 2006, 1256–1259, DOI: **10.1038/sj.cdd.4401962**.
92 C. M. Moon, K. E. Yun, S. Ryu, Y. Chang and D. Il Park, High serum alanine aminotransferase is associated with the risk of colorectal adenoma in Korean men, *J. Gastroenterol. Hepatol.*, 2017, **32**, 1310–1317, DOI: **10.1111/jgh.13684**.
93 M. M. Sohocki, L. S. Sullivan, W. R. Harrison, E. J. Sodergren, F. F. B. Elder, G. Weinstock, S. Tanase and S. P. Daiger, Human glutamate pyruvate transaminase (GPT): localization to 8q24.3, cDNA and genomic sequences, and polymorphic sites, *Genomics*, 1997, **40**, 247–252, DOI: **10.1006/geno.1996.4604**.